PLOS Biology

The ETS transcription factor ELF5 drives lung metastasis in luminal breast cancer via recruitment of Gr-1+CD11b+ myeloid derived suppressor cells

--Manuscript Draft--

Manuscript Number:	
Full Title:	The ETS transcription factor ELF5 drives lung metastasis in luminal breast cancer via recruitment of Gr-1+CD11b+ myeloid derived suppressor cells
Short Title:	ELF5, innate immunity and metastasis
Article Type:	Research Article
Keywords:	Breast cancer; metastasis; luminal A subtype; ELF5; innate immune system; myeloid-derived suppressor cells; MMTV-PyMT.
Corresponding Author:	David Gallego-Ortega Garvan Institute of Medical Research Sydney, NSW AUSTRALIA
Corresponding Author Secondary Information:	
Corresponding Author's Institution:	Garvan Institute of Medical Research
Corresponding Author's Secondary Institution:	
First Author:	David Gallego-Ortega
First Author Secondary Information:	
Order of Authors:	David Gallego-Ortega
	Anita Ledger
	Daniel Roden
	Christina Cho
	Stephanie Louise Allerdice
	Heather J Lee
	Fatima Valdes-Mora
	Adelaide IJ Young
	Brian Young Lee
	Warren Kaplan
	Robert Salomon
	Catherine Piggin
	Brian Rabinovich
	Ewan Millar
	Samantha Richelle Oakes
	Tatyana Chtanova
	Alexander Swarbrick
	Matthew Naylor
	Sandra O'Toole
	Julie MW Gee
	Ian Ellis

	Susan J Clark
	Christopher J Ormandy
Order of Authors Secondary Information:	
Abstract:	Background. During pregnancy, the ETS transcription factor ELF5 establishes the milk-secreting alveolar cell linage by driving a cell fate decision of the luminal progenitor cell. In breast cancer, ELF5 is a key transcriptional determinant of molecular subtype and has been implicated in the development of insensitivity to anti-estrogens, where it becomes essential for renewed cell proliferation. Principal findings. In the PyMT model of luminal breast cancer, induction of ELF5 levels reduced cancer cell proliferation, invasion and motility, associated with a mesenchymal to epithelial transition. Despite these effects, ELF5 greatly increased the size and number of lung metastasis. Myeloid-derived suppressor cells were recruited to the tumor in response to ELF5, and transcriptional programs initiated by established activators of myeloid-derived suppressor cells, such as PDGE and TGFbeta, were induced in cancer cells in response to ELF5. Depletion of myeloid cells using specific Ly6G antibodies prevented ELF5 from increasing metastatic activity. Expression signatures in luminal A breast cancers indicated that increased myeloid cell invasion and inflammation was correlated with ELF5 expression, and increased ELF5 immunohistochemical staining predicted poorer overall survival in the luminal A subgroup. Significance. In the MMTV-PyMT mouse mammary model, increased ELF5 levels drive metastasis by co-opting the innate immune system. Compelling evidence of a similar process in luminal breast cancer patients was found. Thus ELF5 and its pathway provides a new biomarker and a potential therapeutic target for the prevention of disease progression in luminal A breast cancer, characterized by the acquisition of anti-estrogen resistance and metastatic activity, the two defining components of the lethal phenotype.
Suggested Reviewers:	Nancy E Haynes Friedrich Miescher Institute for Biomedical Research nancy.hynes@fmi.ch Expert in animals models of breast cancer. Her career focus has been to understand the epithelial cell interpretation of extracellular signals essential for proper developmental and proliferative responses, with emphasis in the integration of these extracellular signalling to tumour progression. The correct
	William Muller, Professor McGill University william.muller@mcgill.ca Expert in transgenic models of breast cancer, among his contributions to the field is the generation of the MMTV-PyMT model.
	Jeffrey Pollard Albert Einstein College of Medicine jeffrey.pollard@einstein.yu.edu Expert in mechanisms of action of female sex steroid hormones in controlling cell proliferation and on the tumour microenvironment of breast cancer. He has pioneered studies on the role of macrophages and demonstrated that they promote tumour progression and malignancy, with a particular emphasis on metastatic disease.
Opposed Reviewers:	Yibin Kang Princeton University ykang@Princeton.EDU Direct competitor
	Jane Visvader Walter and Eliza Hall Institute visvader@wehi.EDU.AU Current and active collaborator. Presents a conflict of interest.
Additional Information:	

Question	Response
Competing Interests You are responsible for recognizing and disclosing on behalf of all authors any competing interest that could be perceived to bias their work, acknowledging all financial support and any other relevant financial or non-financial competing interests. Do any authors of this manuscript have competing interests (as described in the PLOS Policy on Declaration and Evaluation of Competing Interests)? **If yes**, please provide details about any and all competing interests in the box below. Your response should begin with this statement: *I have read the journal's policy and the authors of this manuscript have the following competing interests:* **If no** authors have any competing interests to declare, please enter this statement in the box: "*The authors have declared that no competing interests exist.*" * typeset	The authors have declared that no competing interests exist.
Ethics Statement You must provide an ethics statement if your study involved human participants, specimens or tissue samples, or vertebrate animals, embryos or tissues. All information entered here should **also be included in the Methods section** of your manuscript. Please write "N/A" if your study does not require an ethics statement. **Human Subject Research (involved human participants and/or tissue)** All research involving human participants must have been approved by the authors' Institutional Review Board (IRB) or an equivalent committee, and all clinical investigation must have been conducted	Mice were maintained following the Australian Code of practice for the care and use of animals for scientific purposes (National Health and Medical Research Council, 2004) observed by the Garvan Institute of Medical Research/St. Vincent's Hospital Animal Ethics Committee (AEC #11/35). The Code requires that animals should be killed in a quiet, clean environment that is away from other animals where possible. As per the recommendations included in the "Guidelines to promote the wellbeing of animals used for scientific purposes" (National Health and Medical Research Council, 2008); euthanasia of mice is performed using CO2 as chemical inhalant followed by cervical dislocation.

according to the principles expressed in the Declaration of Helsinki. Informed consent, written or oral, should also have been obtained from the participants. If no consent was given, the reason must be explained (e.g. the data were analyzed anonymously) and reported. The form of consent (written/oral), or reason for lack of consent, should be indicated in the Methods section of your manuscript. Please enter the name of the IRB or Ethics Committee that approved this study in the space below. Include the approval number and/or a statement indicating approval of this research. **Animal Research (involved vertebrate animals, embryos or tissues)** All animal work must have been conducted according to relevant national and international guidelines. If your study involved non-human primates, you must provide details regarding animal welfare and steps taken to ameliorate suffering; this is in accordance with the recommendations of the Weatherall report, "The use of non-human primates in research." The relevant guidelines followed and the committee that approved the study should be identified in the ethics statement. If anesthesia, euthanasia or any kind of animal sacrifice is part of the study, please include briefly in your statement which substances and/or methods were applied. Please enter the name of your Institutional Animal Care and Use Committee (IACUC) or other relevant ethics board, and indicate whether they approved this research or granted a formal waiver of ethical approval. Also include an approval number if one was obtained. **Field Permit** Please indicate the name of the institution or the relevant body that granted permission.	
Data Availability	Yes - all data are fully available without restriction

PLOS journals require authors to make all data underlying the findings described in their manuscript fully available, without restriction and from the time of publication, with only rare exceptions to address legal and ethical concerns (see the PLOS Data Policy and FAQ for further details). When submitting a manuscript, authors must provide a Data Availability Statement that describes where the data underlying their manuscript can be found. Your answers to the following constitute your statement about data availability and will be included with the article in the event of publication. **Please note that simply stating 'data available on request from the author' is not acceptable.** ***If, however, your data are only available upon request from the author(s), you must answer "No" to the first question below, and explain your exceptional situation in the text box provided.*** Do the authors confirm that all data underlying the findings described in their manuscript are fully available without restriction?	
Please describe where your data may be found, writing in full sentences. **Your answers should be entered into the box below and will be published in the form you provide them, if your manuscript is accepted.** If you are copying our sample text below, please ensure you replace any instances of XXX with the appropriate details. If your data are all contained within the paper and/or Supporting Information files, please state this in your answer below. For example, "All relevant data are within the paper and its Supporting Information files." If your data are held or will be held in a public repository, include URLs, accession numbers or DOIs. For example, "All XXX files are available from the XXX database (accession number(s) XXX, XXX)." If this information will only be available after acceptance, please indicate this by ticking the box below. If neither of these applies but you are able to provide details of access elsewhere, with or without limitations, please do so in the box below. For example: "Data are available from the XXX Institutional Data Access / Ethics	Where indicated, the analysis tools utilising GenePattern software are available at the Garvan hosted GenePattern server http://pwbc.garvan.unsw.edu.au/gp/. Microarray data are available from GEO: GSE58729 [temporary data link: http://www.ncbi.nlm.nih.gov/geo/query/acc.cgi?token=ktkdsywwbbcpjkz&acc=GSE58729.]. This information will only be publicly available after acceptance, this link is for editorial purposes only. All analysis results, additional GSEA gene-sets and custom analysis scripts are available on request from the authors. Any other relevant data are within the paper and its Supporting Information files.

Committee for researchers who meet the criteria for access to confidential data." "Data are from the XXX study whose authors may be contacted at XXX." * typeset	
Additional data availability information:	Tick here if the URLs/accession numbers/DOIs will be available only after acceptance of the manuscript for publication so that we can ensure their inclusion before publication.

384 Victoria Street
Darlinghurst NSW 2010
Australia

t: 61 2 9295 8100
f: 61 2 9295 8101

GARVAN INSTITUTE
Breakthrough Medical Research

Friday, 8 August 2014

Dear Editors of PLOS Biology,

Work from our laboratory has shown that the ETS transcription factor ELF5 is a master regulator of mammary development, causing the mammary progenitor cell to choose a milk-secreting fate (G&D 2008). This progenitor cell is the origin of most breast cancers, and we found that ELF5 is a key determinant of breast cancer subtype, and enables the acquisition of resistance to antiestrogen therapy (PLOS Biol 2012). In the manuscript we are submitting for your appraisal, we show that ELF5 can co-opt the innate immune system, specifically myeloid-derived suppressor cells, to drive metastasis and that this activity occurs specifically within the luminal breast cancer subtype, the same subtype in which ELF5 drives antiestrogen resistance. Luminal breast cancer represents about 2/3 of breast cancers, and disease progression of luminal cancers accounts for around 50% of breast cancer deaths. Our work shows that ELF5 heads a transcriptional pathway driving the progression of luminal cancers to the lethal phenotype. This pathway thus provides a series of new therapeutic targets and prognostic markers. As such this work will be of interest to all breast cancer researchers.

On a more general theme we also show that involvement of the innate immune system can overcome cancer cell intrinsic effects such as a mesenchymal to epithelial transition accompanied by reduced proliferation, motility and invasion. There is a wide spread belief that these effects mitigate against metastasis and our paper resoundingly demonstrates the opposite. The results are very clear- the immune system can swamp these cell intrinsic effects. This aspect of our work will be of great interest to all cancer researchers.

May we suggest Nancy Hynes as the academic editor. Suitable reviewers are William Muller, Montreal; the creator of the PyMT breast cancer model; and Jeffrey Pollard, New York; with a primary focus in the role of macrophages in metastasis.

Yours sincerely

Professor Christopher Ormandy.
Coordinator, Cancer Biology Research Program.

The ETS transcription factor ELF5 drives lung metastasis in luminal breast cancer via recruitment of Gr-1+CD11b+ myeloid derived suppressor cells.

David Gallego-Ortega[1,2]✉, Anita Ledger[1], Daniel Roden[1,2] , Christina Cho[1], Stephanie L Allerdice[1], Heather J Lee[1,3], Fatima Valdes-Mora[1,2], Adelaide IJ Young[1], Brian Y Lee[1] ,Warren Kaplan[4], Robert Salomon[1], Catherine Piggin[1], Brian Rabinovich[5], Ewan Millar[1,6], Samantha R Oakes[1,2], Tatyana Chtanova[1], Alexander Swarbrick[1,2], Matthew Naylor[1,7], Sandra O'Toole[1,7], Julie MW Gee[8], Ian Ellis[9], Susan J Clark[1,2] and Christopher J Ormandy[1,2]✉.

1. *Garvan Institute of Medical Research and The Kinghorn Cancer Centre, 384 Victoria Street Darlinghurst, NSW 2010, Australia.*
2. *St. Vincent's Clinical School of Medicine, Faculty of Medicine, University of New South Wales, NSW, Australia.*
3. *Current address, Epigenetics ISP, Babraham Institute, Cambridge, UK.*
4. *Peter Wills Bioinformatic Center, Garvan Institute of Medical Research, NSW, Australia.*
5. *MD Anderson Cancer Center, Houston, TX, USA.*
6. *Department of Anatomical Pathology SEALS, St. George Hospital, Kogara, NSW, Australia*.
7. *Sydney Medical School, University of Sydney, NSW, Australia.*
8. *Cardiff School of Pharmacy and Pharmaceutical Sciences, Cardiff University, Wales, UK.*
9. *Department of Histopathology, Nottinghan City Hospital and Nottingham University UK.*

✉ *Corresponding Authors*

c.ormandy@garvan.org.au Fax +612 9295 8329 Tel +612 9295 8329

d.gallego@garvan.org.au Fax +612 9295 8329 Tel +612 9295 8340

Running title: ELF5, innate immunity and metastasis.

Abstract.

Background. During pregnancy, the ETS transcription factor ELF5 establishes the milk-secreting alveolar cell linage by driving a cell fate decision of the luminal progenitor cell. In breast cancer, ELF5 is a key transcriptional determinant of molecular subtype and has been implicated in the development of insensitivity to anti-estrogens, where it becomes essential for renewed cell proliferation.

Principal findings. In the PyMT model of luminal breast cancer, induction of ELF5 levels reduced cancer cell proliferation, invasion and motility, associated with a mesenchymal to epithelial transition. Despite these effects, ELF5 greatly increased the size and number of lung metastasis. Myeloid-derived suppressor cells were recruited to the tumor in response to ELF5, and transcriptional programs initiated by established activators of myeloid-derived suppressor cells, such as PDGE and TGFbeta, were induced in cancer cells in response to ELF5. Depletion of myeloid cells using specific Ly6G antibodies prevented ELF5 from increasing metastatic activity. Expression signatures in luminal A breast cancers indicated that increased myeloid cell invasion and inflammation was correlated with *ELF5* expression, and increased ELF5 immunohistochemical staining predicted poorer overall survival in the luminal A subgroup.

Significance. In the MMTV-PyMT mouse mammary model, increased ELF5 levels drive metastasis by co-opting the innate immune system. Compelling evidence of a similar process in luminal breast cancer patients was found. Thus ELF5 and its pathway provides a new biomarker and a potential therapeutic

target for the prevention of disease progression in luminal A breast cancer, characterized by the acquisition of anti-estrogen resistance and metastatic activity, the two defining components of the lethal phenotype.

Introduction

Breast cancer is characterized by heterogeneity in its patterns of clinical course, histological appearance, gene expression and genetic alterations. Clustering methods can reduce this complexity by recognizing the common patterns that group tumors into subtypes. The patterns of genetic lesions are distinct across subtypes, but common within them, and gene expression and clinical behavior are similarly distributed, indicative of a shared path to cancer within subtypes, and different paths across them [1]. The most striking subtype distinction in breast cancer was recognized before the genomic era. The levels and proportion of estrogen receptor (ER) in cancers divides breast cancer into two very different diseases, recognizable by more than their response to antiestrogen therapies. For example, the risk of recurrence remains constant across survival time for ER+ disease, but drops dramatically after 5 years for ER- disease [2,3]. ER+ disease is also notoriously insensitive to chemotherapy [4-6]. The basis for this stark dichotomy probably rests in the developmental events influencing the phenotype of the luminal progenitor cell pool, whose members are thought to be the cell of origin for the ER- basal and ER+ luminal breast cancer subtypes [7]. The ETS transcription factor ELF5 plays a key role in the decisions made by these progenitor cells.

During normal development ELF5 participates in the regulation of the stem and progenitor cell hierarchy [8-10], where it is first expressed as mammary stem cells differentiate to become progenitor cells [11,12]. In progenitor cells an additional rise in ELF5 levels, in response to progesterone and prolactin, and paracrine signal including RANKL [13,14] and Wnt family

members [15]; force a cell fate decision that establishes the secretory cell linage responsible for milk production during pregnancy [8,16]. An alternative progenitor cells fate, that of an ER+ hormone sensing cell, may result if ELF5 levels remain in check due to the dominance of the estrogen-driven phenotype. In the cells of the mouse mammary gland ELF5 exhibits a mutually exclusive IHC staining pattern with estrogen and progesterone receptors [8,13]. Knockout of ELF5 using K14CRE caused the loss of epithelial patterns of gene expression, resulting in an epithelial to mesenchymal transition within the mammary gland [11].

In luminal breast cancer cells a mutual negative-regulatory loop between ER and ELF5 occurs, that is dominated by ER and so keeps ELF5 levels low [17]. Conversely, ER- basal and HER2+ breast cancers are characterized by high ELF5 levels, while the stem cell-like and highly mesenchymal claudin-low subgroup, does not express *ELF5* [17]. Knockdown of ELF5 levels in luminal breast cancer cells has a small effect on proliferation, but a much greater effect is seen in basal cell lines [17]. Constitutive induction of ELF5 levels in breast cancer cells results in a mesenchymal to epithelial transition (MET) while knockdown has the opposite effect [11,17]. Importantly, ELF5 levels rise when MCF7 luminal breast cancer cells acquire antiestrogen resistance. Resistant cells become dependent on ELF5 for their proliferation [17]. Thus increased ELF5 levels provides an escape pathway from inhibition of proliferation by antiestrogen therapy [9], facilitating disease progression. Whether ELF5 is involved in other key aspects of disease progression, such as metastasis, is unknown.

Like primary tumor formation, the acquisition of the metastatic phenotype involves both cell-intrinsic events that alter cell phenotype and cell-

extrinsic events, such as interactions with the host environment. An example of an intrinsic event is the gain of phenotypic plasticity, such as epithelial to mesenchymal transition (EMT), and its reverse MET, which respectively confer and remove invasive and motile characteristics to cancer cells. For example, in the MMTV-PyMT mammary cancer model [18-20], expression of Myc caused an EMT [21]. An example of an extrinsic event in this model is the tumor's ability to interact with the innate immune system to assist with metastasis. For example, knockout of CSF-1 depleted macrophages delayed the development of lung metastases, while over expression caused the migration of macrophages into the tumor and accelerated metastasis [22]. When macrophage chemotaxis toward CSF-1 was ablated by deficiency of the Wiskott-Aldrich Syndrome protein, the metastasis promoting effect of macrophages was lost [23]. Another important innate immune cell subset active in metastasis of mammary and breast cancer are myeloid derived suppressor cells (MDSC) [24]. Their circulating numbers are increased by the presence of a tumor [25,26]. They invade primary tumors where they promote angiogenesis, via MMP secretion and VEGF production, and become component cells of the new endothelial layer [27]. These cells inhibit and kill natural killer cells [28] and T- lymphocytes [29], while promoting the proliferation of the T-regulatory cell population and inhibiting dendritic cell maturation; all mechanisms that allow tumors to evade immune control [30]. They also promote type II macrophage development and so can promote macrophage-assisted metastasis. In the PyMT model of mammary metastasis, increased TGF beta signaling caused their recruitment to primary tumors. Depletion of their numbers reduced the number of lung metastases while tumor cell co-inoculation with MDSC increased the number of lung metastases [31,32].

We have used our inducible mouse model of mammary-specific ELF5 expression, in the context of luminal mammary tumors induced by PyMT expression, to investigate the intrinsic and extrinsic roles played by ELF5 during mammary carcinogenesis and progression to metastatic disease.

Results

Effects of ELF5 on primary tumorigenesis.

The transgenic mouse model constructed for this study is shown in Figure 1A. Triple-transgenic animals were created carrying one copy of each of the alleles on an inbred FVB/N genetic background. Administration of Doxycycline (DOX) induces expression of a single mRNA encoding human *ELF5* and enhanced green fluorescent protein (EGFP), separated by an internal ribosome entry site (IRES) allowing independent translation. The *PyMT* oncogene is independently and constitutively expressed in the mammary gland from the *MMTV* promoter. Dox was administered from 6 weeks of age (chronic scenario) to induce *ELF5* expression during carcinogenesis, or after tumors had formed, from 11-12 weeks of age (acute scenario). Time course experiments (Fig. 1B) showed that 7 days after the administration of DOX in the feed, the ELF5 protein was detectable by western blot in established mammary tumors (Fig. 1B). Induction of ELF5 was maintained in established tumors formed in mice continuously treated with Dox from 6 weeks of age (Fig. 1B chronic ELF5). Acute induction of ELF5 caused discrete regions of tumor hemorrhage to occur, while chronic induction resulted in wide-spread tumor hemorrhage, in both cases characterized by erythrocytes within the affected area of the tumor and macrophages exhibiting hemosiderin.

Infiltrating CD45+ hematopoietic cells were found associated as clusters or along the basement membrane planes between lobular structures (Fig. 1C). Chronic induction of ELF5 caused higher vascular density, with a finer and more branched vasculature forming. Quantification of CD31 staining for endothelial cells reflected this (Fig 1D), with greater numbers of blood vessels counted per field. This was quantified by flow cytometry using enzymatically disaggregated tumors experiencing either acute or chronic induction of ELF5 (Fig. 1E). A massive increase in tumor erythrocytes was measured in both scenarios. The numbers of endothelial cells increased in the tumors experiencing chronic forced ELF5 induction. CD45+ leukocyte invasion of the tumor was also clear in the chronic scenario.

Examination of ELF5 induction via EGFP fluorescence of whole tumors showed a heterogeneous pattern of expression (Fig. 2A). This was seen under either acute or chronic scenarios and may result from chimeric expression patterns of the *rtTA* transgene, a feature of older MTB mice [33]. We used Kaplan-Meier survival analysis to analyze primary tumor growth using chronic administration of DOX. Only mice that showed a tumor burden of 8-12% of body weight at autopsy were included in the analysis and there was no difference in tumor burden between the experimental groups (Fig. 2B). Overall survival at 10% tumor burden showed no significant difference (Fig. 2C), however, time to tumor detection was 10 days shorter and the time from tumor detection to 10% tumor burden was 10 days longer with induction of ELF5. Although statistically significant these effects are modest. To overcome the confounding effects of heterogeneous ELF5 induction (Fig. 2A), we FACS-sorted tumor cells (Lin- and CD24+) from chronically DOX-treated animals and captured those that were

EGFP+, then injected them into the mammary ducts of FVB/N host animals pretreated with DOX. These transplants resulted in longer overall survival, longer time to tumor detection and longer time to the ethical endpoint, than cells similarly sorted and injected but from animals not carrying the *ELF5* transgene (Fig. 2D). When tumor cells were made fluorescent by 7 days of DOX administration, flow sorted to capture EGFP+ cells as before, and then injected into the mammary ducts of hosts treated with or without DOX, EGFP+ cells again produced slower growing tumors compared to similarly sorted WT cells, or to EGFP+ cells injected into animals without DOX administration (Fig. 2E). The two control groups (WT and EGFP+ no DOX after transplant) produced tumors that expanded at indistinguishable rates.

Using a BrdU pulse to label cells in S-phase we observed that much higher rates of cell proliferation occurred in the areas of the tumor which expressed low levels of ELF5, marked by low or no EGFP. This was observed in both acute (Fig. 3A) and chronic (Fig. 3B) scenarios. We examined cell motility in a Boyden chamber assay using flowcytometric cell sorting to procure EGFP+ and WT cells from chronically-induced tumors. Induced Elf5 reduced cell motility through the membrane towards the serum containing media (Fig. 3C). When we added matrigel to the top surface, forcing cells to degrade it before moving through the membrane, we found a similar result (Fig. 3D, left panel). These results were also found using a PyMT cell line carrying a Doxycycline-inducible *ELF5* expression vector (Fig. 3D, right panel). When we injected equal numbers of EGFP+ or WT cells from disaggregated tumors into the tail vein of FVB/N hosts we observed far fewer colonies of cells in the lungs (Fig 3E).

Affymetrix Arrays were used to transcript profile mRNA expression of flow-purified cells in triplicate. We used SES analysis [17,34] to determine if induction of ELF5 altered the molecular subtype of PyMT tumours. Whether PyMT tumors better model human luminal A or B is not clear and so p values for both are presented. In the acute scenario, where the tumor formed prior to induction of ELF5 for 2 weeks, luminal PyMT cells lost claudin-low subtype patterns of expression and became more like the basal subtype (Fig. 3F). In contrast, in the chronic scenario, where carcinogenesis occurred in the context of ELF5 induction, the PyMT tumors gained claudin-low subtype expression patterns (Fig. 3G). Acute induction of ELF5 in mouse mammary tumors (Fig. 3H), or in the highly mesenchymal and profoundly ELF5- MDA-MB-231 cell line (sFig. 1), caused a pronounced shift in gene expression consistent with a mesenchymal to epithelial transition. Chronic induction of ELF5 produced a muted effect (Fig. 3H, overlaps Fig. 3I). We used gene set enrichment analysis to further investigate the differences between the acute and chronic scenarios. The differential effects on the claudin-low subtype, mesenchymal phenotype and EMT shown in Figure 3 were clearly apparent in our Cytoscape visualization of this data (sFig. 2, expanded view sFig. 3). The major difference revealed by this analysis was positive enrichment in the chronic scenario, and negative enrichment in the acute scenario, of a cluster of gene sets representing breast cancer stem cell populations (sFig. 3). Thus the shift towards the claudin-low subtype in the chronic scenario is associated with enhanced expression of a stem-cell signature, while the shift away from the claudin low subtype in the acute scenario is associated with the suppression of stem cell characteristics.

Effects of ELF5 on metastasis

We examined the effect of the induction of ELF5 on the metastatic behavior of the PyMT model. In control animals, constitutive PyMT expression produced no visible lung metastatic nodules by the time the primary tumors reached the ethical endpoint of 10% body weight (Fig. 4A), but small metastases within the lung were detectable by H&E histology (Fig. 4B). DOX administration in control animals had no effect on metastasis (Fig. 4C and D). Chronic induction of ELF5 resulted in a dramatic increase in metastasis to the lungs, now visible as numerous nodules on the surface of the lung at the ethical endpoint (Fig. 4E) and large and numerous metastases within the lungs by H&E histology (Fig. 4F). Acute induction of ELF5 also increased lung metastases (Figs. 4G and 4H). These metastases all expressed ELF5, observed by visualisation of EGFP (Fig. 4I) and by ELF5 IHC (Fig. 4J). Quantification showed a positive correlation between the size of the metastatic lesion and the level of ELF5 by IHC (Fig. 4K). Unlike the primary tumors the metastases showed no regions of hemorrhage. Quantification of H&E stained sections showed statistically significant increases in the number and area of lung metastases with chronic or acute induction of ELF5 (Figs. 4L and M) that were similar to the metastasis-promoting effects of pregnancy in this model (Fig. 4N). Measurement of metastatic area produced similar results (Fig. 4O). Chronic induction of ELF5 greatly increased the amount of PyMT-mRNA present in blood (Fig. 4P).

Effects of ELF5 on the gene expression profiles of primary tumor and metastases.

We purified EGFP+ mammary cancer cells from enzymatically disaggregated primary tumors and lung metastases, produced using the chronic

scenario, and examined their global patterns of gene expression compared to WT cancer cells using Affymetrix arrays, with visualization by GSEA and Cytoscape. In primary cancers, EGFP+ cells were compared to WT cells to discover functions altered by ELF5 induction during carcinogenesis, shown by the inner node color, while the outer node shows how these functions changed again after metastases (Fig. 5). A fully scalable .pdf is available as sFig. 4. Functions related to cell cycle control, DNA repair, transcription, and translation were suppressed by ELF5 during primary carcinogenesis and remained similarly suppressed in the metastases. Aspects of kinase-based cell signaling were increased by ELF5 during primary carcinogenesis but were then generally suppressed following metastases, although GPCR mediated signaling increased during carcinogenesis and increased again following metastasis. The metastases showed a shift away from the claudin-low subtype by SES analysis (inset), with little change in the EMT gene expression signature (bottom heat map), but a loss of stem cell gene expression signatures by GSEA (sFig. 5). Inflammation, immune system, hypoxia and interferon responses, which were all enriched in the primary tumors, in response to ELF5 were all suppressed in the metastases. Thus the metastases show continued proliferation but loss of kinase signaling accompanied by loss of inflammation and stem cell characteristics. The metastases exhibit a different molecular phenotype compared to the tumors that produced them.

Mechanisms driving metastasis

There is an extensive and persuasive literature regarding the pro-angiogenic and -metastatic roles of innate immune cells in the PyMT model. We examined tumor immune cell infiltrates, reasoning that ELF5 may drive the

production of factors that recruit and activate innate immune components. We used flow cytometry to analyse the immune cell subsets within tumors that developed under the chronic scenario. We gated-out red blood cells and measured myeloid (Fig. 6A) and lymphoid (Fig. 6B) immune cells as a percentage of the remaining total cells, or as a proportion of total CD45+ hematopoietic cells. Supplementary figure 6 shows the gating strategy used to produce this analysis. Among the myeloid populations, MDSCs (defined as Gr-1+CD11b+) showed an increased proportion of either total cells or hematopoietic cells. T- and B-cell lymphoid lineages increased as a proportion of total cells, and when expressed as a proportion of hematopoietic cells we observed a 1.5 fold increase in B cells and a 2-fold decrease in the proportion of CD8+ T-cells cells. CD8+ T cells are killed by activated MDSC, suggesting this was occurring in response to ELF5.

To determine if the increase in MDSC could account for the increase in metastases caused by ELF5 we used the specific Ly6G antibody, to deplete the MDSC population during acute induction of ELF5 in established tumors. The depletion was very effective, no MDSCs were observed in the blood of Ly6G-treated animals (Fig. 6C). After 2 weeks this treatment halved the number of lung metastases that occurred in response to acute induction of ELF5 (Fig. 6D), but did not ablate metastasis. We also observed that the antibody treatment reduced the number of red blood cells within the primary tumor (Fig. 6E), establishing MDSCs as a key part of the mechanism responsible for both induction of metastases and the hemorrhagic tumor phenotype by ELF5.

<u>Effects of ELF5 on breast cancer phenotype and survival.</u>

We clustered the TCGA breast cancer cohort into intrinsic subtypes using the PAM50 classifier, and for each subtype we produced a ranked gene list by correlation to *ELF5* expression level. This ranked list was used as the input for GSEA, to discover the subtype-specific functions that correlated with *ELF5* expression. We concentrated on the luminal subtypes given the luminal classification of the PyMT model and the results are presented as a Cytoscape visualization (Fig. 7). A scalable version is available as sFig. 7 and the full appearance of the network is shown in Fig. 7A, with yellow nodes indicating the subnetwork presented in Fig. 7B. Higher *ELF5* expression in luminal breast cancers was correlated with a shift away from luminal characteristics toward basal characteristics. Stem and progenitor cell signatures became more prominent, as did mesenchymal signatures, and a shift towards the claudin-low subtype occurred. Estrogen responsiveness was reduced in tumors with high *ELF5* expression, while signatures showing immune system involvement, interferon response, the presence of monocytes and inflammation were all enriched with higher *ELF5* expression.

During normal mammary development monocytes are recruited to the mammary gland in response to pregnancy, lactation and weaning, where they participate in tissue remodeling events. We assembled a number of gene sets providing expression-signatures of lactation and involution, and examined their enrichment in the PyMT model in response to induction of ELF5, and in the TCGA series in correlation with *ELF5* expression. Forced *ELF5* expression in the PyMT model induced the expression of lactation and involution signatures. The same effect was apparent in the luminal A breast cancers where expression of lactation and involution signatures correlated with the level of *ELF5* expression (Fig. 7C).

No correlation was observed in luminal B cancers. A number of factors secreted by tumor cells are known to recruit MDSCs to the tumor. We assembled a gene set comprising these factors and examined its expression in response to the induction of ELF5 in PyMT mice. The geneset, which includes factors such as *PTGS2*, *TNF*, *VEGFA*, *M-CSF*, *G-CSF*, *TGFB1* and *KITLG* (sFig. 8A), was enriched by gene set enrichment analysis in both chronic and acute scenarios (sFig. 2). Interestingly this induction was reversed in the metastases. We searched for transcriptional signatures indicative of the action of the most differentially expressed genes in the set (sFig. 8B). This revealed a robust transcriptional response-signature to PTGS2, VEGF, TGFB and KITLG, the four most differentially expressed factors for which we could identify an appropriate response gene set. The alteration in the expression of these signatures was seen with acute and chronic ELF5 induction, but was very much reduced in the metastases. We searched for evidence that these transcriptional signatures were correlated with *ELF5* expression in luminal breast cancers using GSEA (sFig. 8C). Luminal A breast cancers showed robust signatures indicative of PTGS2, VEGF and TGFB action that was correlated with *ELF5* expression. No enrichment of SCF/KIT action was found. These observations demonstrate that *ELF5* expression produces a primary tumor microenvironment enriched for PTGS2, VEGF and TGFB activity in both mouse and human mammary cancers, providing a potential molecular mechanism for MDSC recruitment. These observations suggest that the immune system of a patient with a luminal A breast cancer expressing high ELF5 levels receives signals mimicking a lactating and involuting mammary gland, and it responds by providing monocytes to the breast to facilitate tissue remodelling, however, in the context of immortal and cancerous mammary

epithelial cells secreting factors such as those above that are capable of activating MDSCs, this process leads to participation of these cells in metastasis.

We stained a cohort of luminal ER+ HER2- tumors [35] for ELF5 protein levels (Fig. 8). All patients were treated with the antiestrogen Tamoxifen and none received chemotherapy. We observed nuclear and cytoplasmic patterns of ELF5 staining. Across all ER+ cancers higher nuclear staining predicted better overall survival ($p=0.04$ Fig. 8A) while higher cytoplasmic staining predicted worse survival ($p=0.06$). These same effects were evident for distant metastasis free survival (Fig. 8B) but with larger p values. We used the St Gallen definition of Ki67% to split these ER+ cancers into luminal A and B tumors [36]. We found that within the luminal A subgroup higher nuclear ELF5 staining showed a trend toward predicting better overall survival (Fig. 8A) while cytoplasmic staining predicted poorer survival ($p=0.03$) with a large hazards ratio of 2.9. A similar effect was evident for distant metastasis free survival (Fig. 8B). In contrast ELF5 levels had no predictive value for survival in the luminal B subtype. In the Nottingham ER+ cancers nuclear ELF5 levels were higher in patients with local or regional recurrence, with lower proliferation or mitosis or with tubular differentiation. Higher cytoplasmic ELF5 occurred in cancers with poorer Nottingham Prognostic Index [37], in lobular cancers, and with higher mitosis (sTable 1).

Discussion

We show that induction of ELF5 in the PyMT model leads to a massive increase in lung metastasis, despite reducing primary tumor proliferation and

inducing MET, because ELF5 recruits MDSCs to assist metastasis. Analysis of human breast tumor data indicated that these processes also operate in humans. It is likely that ELF5-driven release of factors responsible for MDSC recruitment mimic mammary involution, and so activate the normal host immune response for mammary tissue remodelling. Given the previously described role of ELF5 in the progression to antiestrogen insensitivity in luminal breast cancer, where ELF5 levels rise [17], and the now documented effects of increased ELF5 levels on metastasis, ELF5 is emerging as a major driver of disease progression to the lethal phenotype in luminal A breast cancer.

Hemorrhagic necrosis and intratumoral hemorrhage is observed in breast cancer [38], where it generates pain due to mastodynia in otherwise painless cancers. Acute induction of ELF5 in the mouse provides a good representation of the human pathology, where isolated hemorrhagic regions are seen. The basis for hemorrhage is likely two fold; firstly MDSC contribute to the phenotype, as shown by its reduction following suppression of these cells with Ly6G antibody. This contribution is likely to be due to the direct participation of MDSC progeny in the vessel walls, leading to finer and leaky vessels, but this remains to be demonstrated by fate mapping. Secondly ELF5 induces VEGF expression, and a robust VEGF response signature was found, indicating that vasculogenesis could be stimulated directly by ELF5 via this well-established pathway.

ELF5 has been proposed as a metastasis suppressor gene [11]. Knockdown of ELF5 in luminal T47D cells resulted in an epithelial to mesenchymal transition, while induction of ELF5 in the claudin-low MDA-MB-231 cell line caused the reverse mesenchymal to epithelial transition. Results from our laboratory support this finding, with knockdown of ELF5 in the basal

HCC1937 cell line producing a more mesenchymal and claudin-low phenotype, and induction of ELF5 in luminal MCF7 cells producing a less mesenchymal and claudin-low phenotype [17]. Acute induction of ELF5 caused PyMT tumors to shift their molecular subtype to become more basal like and less like the claudin low subtype, and transcript profiling showed a mesenchymal to epithelial transition was the likely cause of this. Chronic induction of ELF5 caused PyMT tumors to become more claudin-low like and the enrichment of stem cell signatures was the likely cause. Functionally, constitutive over expression of *ELF5* in claudin-low MDA-MB-231 cells made them less invasive in *in vitro* assays and reduced seeding to lung when injected via the mouse tail vein [11] and we also produced these results, using an inducible system. Our results diverge from those of Chakrabarti and colleagues in the luminal PyMT system. Using a cell line derived from a PyMT mouse mammary tumor, showing 250-fold constitutive over expression of ELF5, no significant difference in *in vitro* proliferation, xenografted primary tumor volume or the incidence of lung metastasis was seen, but a reduced number of metastatic lung surface nodules was reported [11]. We show, in an *in situ* and *in vivo* model of carcinogenesis, that ELF5 drives metastasis in the PyMT model, via engagement of the innate immune system and despite the mesenchymal to epithelial transition it produces. We suspect that the cell line used by Chakrabarti and colleagues may not represent the luminal subtype, as it has been forced to adapt in tissue culture to constitutive and very high ELF5 expression, conditions we have demonstrated to shift cells away from the luminal molecular subtype [17]. Knockout of ELF5 in the Neu mouse model of HER2+ breast cancer caused an increased number of lung nodules [11]. We show that the effects of ELF5 on inflammation and monocyte invasion are

restricted to the luminal A subtype in the TCGA series. Thus the actions of ELF5 are subtype specific and so luminal models must be used to infer responses in luminal subtypes. The epithelializing effect of Elf5 has been consistently reported numerous times (Chakrabarti et al., Kalyuga et al. and this report), but only in the *in situ* developed tumors experiencing induction of ELF5 was the effect of ELF5 on the innate immune system seen.

Thus while ELF5 may act as a metastasis suppressor gene in the ER- and estrogen insensitive breast cancer subtypes, we conclude that in the estrogen sensitive luminal A subtype increased Elf5 expression provides a path to metastasis via innate immune system recruitment, as well as a path to resistance to antiestrogen therapies [17]. As such, elevated ELF5 levels may be a principal determinant of disease progression in luminal A breast cancer.

Materials and Methods.

Experimental animals**.**

Mice were maintained following the Australian code of practice for the care and use of animals for scientific purposes observed by the Garvan Institute of Medical Research/St. Vincent's Hospital Animal Ethics Committee (AEC). The Elf5 inducible PyMT mammary tumour transgenic model has been generated by crossing the MMTV- Polyoma Middle T antigen (PyMT) mouse mammary tumour model (Guy et al. 1992) with the doxocyclin (Dox) inducible Elf5 Knock In mouse line (Oakes 2008). The inducible promoter induces a bicistronic cassette codifying for the human version of Elf5 followed by eGFP using an IRES sequence. We used the rtTA locus under the MMTV promoter to control the

expression of Elf5 in the mammary epithelial cells (MTB animals). All animals used in this study are heterozygous for Elf5, MTB and PyMT. Supplementary Figure 1A shows a schematic representation of the transgenic cassettes and genotypes used for the study. To induce the expression of the Elf5 and EGFP mice were exposed to a diet containing 700mg/Kg of Doxocyclin (Gordon's Specialty Stockfeeds). For the neutrophil depletion experiment, 100µg of Ly6G antibody clone 1A8 (UCSF) was injected IP twice a week for 2 weeks, a pretreatment injection was performed 2-3 days before Dox exposure. Lung seeding experiments were performed by injecting ($5x10^4$ cells in 100µl of saline) by the vein of the tail of FVB/N congenic hosts (PyMT cells) or NSG (JAX) immune-deficient mice for MDA-MB-231 cells. Orthotopic trasplantation of mammary cells were performed by intraductal injection of $8x10^4$ cells into the main duct of the 4^{th} mammary gland. Luciferine substract was injected IP at 15mg/ml (100µl/mouse) and luminescence read was taken 10 minutes later using the IVIS Lumina instrument (Xenogen).

Cells and constructs.

Elf5 was tagged at the 3' end with V5 and incorporated into the pHUSH-ProEX vector as descried before [17]. Elf5 expression was achieved using Doxycycline (Clontech) at 0.1µg/ml. Luciferase encoding and pHUSH-ProEx plasmids were packed into retrovirus using PlatinumE cells (Cell Biolabs) using FuGene6 or X-Treme transfection reagent (Roche) following manufacturer instructions.

Flow cytometry and antibodies.

DAPI ([4',6-diamidino-2-phenylindole dihydrochloride]) (Molecular Probes)

was used as death cell exclusion marker. Flow cytometry was performed using the following fluorophore conjugated antibodies: CD45, CD31, Ter119 from BD Pharmingen; CD3 (clone 17A2), F4/80 (clone BM8), Gr-1 (clone RB6-8C5), CD4 (clone GK1.5), CD8 (clone53-6.7), CD11c (clone N418), CD11b (clone M1/70) and B220 (clone RA3-6B2) from eBioscience. For neutrophil depletion experiments Ly6G antibody was used (UCSF) and FACS performedusing an anti-rat IgG secondary form Biolegends. A list of the defined populations using these antibodies is listed in sFig6A.

Gene expression profile analysis and bioinformatics

Normalization and probe set summarization was performed using the robust multichip average [39] implemented in the Affymetrix library [40] from R [41] as part of the *NormalizeAffymetrixST* module in GenePattern. For all pair-wise experimental comparisons, Gene Set Enrichment Analysis (GSEA) [42] was run in pre-ranked mode using a ranked list of the Limma moderated t-statistics. The effect of ELF5 perturbation on the enrichment and change in breast cancer molecular subtype was measured using subtype expression score (SES) analysis, as described previously [17,34]. Where indicated, the analysis tools utilising GenePattern software [43] are available at the Garvan hosted GenePattern server http://pwbc.garvan.unsw.edu.au/gp/. Microarray data are available from GEO: GSE58729 [temporary data link: http://www.ncbi.nlm.nih.gov/geo/query/acc.cgi?token=ktkdsywwbbcpjkz&acc=GSE58729.]. All analysis results, additional GSEA gene-sets and custom analysis scripts are available on request from the authors.

The Cancer Genome Atlas database.

For the analysis of TCGA expression data, clinical and molecular annotation of samples was obtained from the Cancer Genome Atlas (TCGA) breast cancer publication [44]. Agilent mRNA expression microarray data (Level 3) was obtained from the TCGA data portal in January 2012. Missing expression values were imputed and replaced using the k-nearest neighbor (KNN) approach, with k=10 (using the *ImputeMissingValuesKNN* module in GenePattern). The TCGA microarray data consisted of a total of 533 tumours. From this, we generated 4 subsets of patients: 98 with a basal-like PAM50 molecular sub-type; 231 with a Luminal A PAM50 sub-type; 127 with a Luminal B PAM50 subtype; and a combined Luminal (A and B) set of 358 tumour samples.

The samples in each of these 4 subsets and the set of all 533 patients, were each stratified on expression level of ELF5 and the top 25% ($ELF5^{hi}$) and bottom 25% ($ELF5^{lo}$) expressing samples were selected. For each of these ELF5 stratified groups, differential gene expression between $ELF5^{hi}$ and $ELF5^{lo}$ patient groups was assessed, for each gene, using an empirical Bayes, moderated t-statistic implemented in Limma [45] via the *limmaGP* tool in GenePattern.

Gene Set Enrichment Analysis (GSEA).

1000 gene-set permutations were performed using minimum and maximum gene-set sizes of 15 and 1500, respectively. Gene-sets used in GSEA were extracted from version 4.0 of the Broad institute's Molecular Signatures Database (MSigDB) [46] and extended with additional curated gene-sets from

literature. All GSEA analysis was performed using a combined set of the c2, c6 and c7 gene-sets from MSigDB plus additional curated sets that we identified in the literature. Network-based visualization and analysis of the GSEA results was carried out using the *Cytoscape* [47] *Enrichment Map* [48] plug-in, with permissive thresholds of: FDR (Q-value)=0.25; P-value=0.05 and overlap coefficient cutoff=0.5.

SES.

Briefly, Elf5 associated gene-signatures were generated from the PyMT transcript profiling using inclusion thresholds of FDR<0.05 and fold-change of 1.5. These were then used to calculate an expression signature score for each sample in the human breast cancer UNC337 expression dataset [49]. A higher score indicates that the breast cancer sample is more positively correlated with the Elf5 expression signature. Subtype expression signature scores, s, are calculated as follows,

$$s = \frac{\sum_g x_g y_g}{\sum_g |x_g|}$$

where the sum is over all genes, g, in the Elf5-derived expression signature set, x_g is the log2-fold-change for that gene from the Elf5 signature data and y_g is the log2-expression for the same gene in the UNC337 sample. Non-matching gene symbols were discarded and for each gene only the probe with highest expression level was used [34]. The UNC337 samples were then stratified into 6 predicted molecular subtypes and p-values calculated between each using the Wilcoxon-Mann-Whitney test. For each Elf5 signature the number of matching genes identified in the UNC337 cohort is listed in the text where applicable.

RNA expression analysis..

RNA extraction was performed using the RNeasy extraction kit (Qiagen) following manufacturers procedure. For blood samples, Trizol (Ambion, Life technologies) lysis was performed before kit purification. High-Capacity cDNA Reverse Transcription Kit (Applied Biosystems) was used for the cDNA preparation. Quantitative PCR was performed using the LightCycler480 (Roche) using SYTO9 as a dye and the $2^{-\Delta Ct}$ method to analyse expression difference [50]. Q-PCR PyMT in blood was detected using the following primers: Fwd: tgtgcacagcgtgtataatcc and Rv: tcatcgtgtagtggactgtgg; and confirmed with Fwd: taagaaggctacatgcggatgggt and Rv: ggcacctggcatcacatttgtctt; and housekeeping gene GAPD using the following primers Fwd: agcttgtcatcaacgggaag; and Rv: tttgatgttagtggggtctcg. Q-PCR for Elf5 was detected using Taqman probe Mm00468732_m1 or Hs01063022_m1 (Applied Biosystems), and housekeeping gene GAPD, Mm99999915_g1 or Hs99999905_m1; using the 7900H Fast Real-Time PCR system (Applied Biosystems).

Immunohistochemistry and immunoblot.

For ELF5 and GFP immunohistochemistry, slides were blocked with protein block after antigen retrieval using Dako buffers (pH 6.1 at 125C for 2min, or pH9 at 100C for 25 min), followed with 0.05%Tween in PBS or 0.2% TritonX100. Primary antibodies were incubated for 1 hour, ELF5 1:500 (N20, sc-9645, Santa Cruz) or GFP 1:200 (A11122, Invitrogen), then followed by either Rabbit anti-Goat 1:100 (Invitrogen) and LSAB+ label (Dako) or Envision Rabbit 30min (Dako), then detection with DAB+ (Dako). For ELF5 IHC in patient samples, following blocking of the 4 micron paraffin-embedded sections from breast

cancer TMAs for endogenous peroxidases, antigen retrieval was performed using pressure cook-microwaving in EDTA buffer (ph9) for 5 mins. This was followed by 0.02% Tween in PBS blocking for 5 mins. Primary antibodies were incubated overnight with ELF5 antibody 1:70 in 0.1% BSA.PBS (N20 sc-9645, Santa Cruz) at room temperature. Detection was performed using 1:1000 Rabbit anti-Goat in 0.1% BSA.PBS (Invitrogen A10537) for 20 mins, followed by Envison+ system-HRP labelled polymer anti-rabbit for 20 mins (Dako 4003). DAB chromogen solution (Dako) was applied for 6 mins followed by methyl green counterstaining. ELF5 nuclear and cytoplasmic staining assessment was performed using H-Score analysis that encompasses both percentage positivity and staining intensity on a 0-300 scale.

GFP and BrdU co-immunofluorescence antigen retrieval was pH 9 and 100°C for 25 minutes, followed by 0.2% TritonX100 then 1:250 GFP (A11122, Invitrogen), and 1:200 BrdU (M0744, Dako) at 4°C overnight. This was followed by 30min incubation with AlexaFluor 488-tagged anti-rabbit antibody, AlexaFluor 555-tagged anti-mouse antibody (1:200; Invitrogen) and ToPro (1:2000; Invitrogen).

Protein analyses by Western Blot were done as previously described [17]. Primary Antibodies used were anti-β-actin (AC-15, Sigma), anti-ELF5 (N20, sc-9645, Santa Cruz) and anti-V5 (R960-25, Invitrogen).

Cell culture and plasmids:

MDA-MB-231 and PyMT cells were maintained in RPMI (Gibco) supplemented with 10% Tet free FBS (Clontech), 10mM HEPES (Gibco) and 0.25 IU/ml of insulin (Novo Nordisk) in standard culture conditions of 37ºC, 5% CO_2

and 95% humidity. PyMT tumour cells were established in culture from enzymatically disaggregated PyMT tumours and double FACS-purification based on CD24 expression. MDA-MB-231 and PyMT cell lines were stably transduced with an inducible Elf5 system (pHUSH-ProEx, Genentech) [51].

In vitro invasion assays.

Boyden Chamber assays (Bencton Dickinson) were performed by plating $4x10^4$ cells (MDA-MB-231) or $1x10^5$ cells (PyMT) in media containing 0.5% FBS, the chemotactic gradient was established by placing the insets into full media (10%FBS) containing wells. Invading cells were visualized with the Diff Quick Stain Kit (Lab Aids). Area measured with Image J 1.41 (Wayne Rasband, US National Institutes of Health). Wound healing assays were performed by scratching confluent monolayers of MDA-MB-231 cells in the presence of Mitomycin C and followed over 36h.

Flow cytometry:

Flow cytometry was performed using FACS Canto II (analysis) and FACS Aria III (sorting) from Becton Dickinson and exported to the FlowJo software (Tree Star Inc.) for data analysis.

Statistical analyses:

Sample comparisons have been made by unpaired T-Test using the GraphPad Prism software, La Jolla California USA. All error bars showed in this paper correspond to standard error unless otherwise stated.

Patient samples description:

The patient cohort is a subset of the Nottingham series [35] comprising Luminal ER+ patients treated with tamoxifen but no chemotherapy, the distinction of luminal A or luminal B subtype was made according to the St Gallen criteria: n=126 versus survival (74 luminal A, 52 luminal B); n=129 versus DMFS (76 luminal A, 53 luminal B). Optimal staining cutpoints for analysis were selected using Xtile.

Acknowledgments

We thank Pauline Finlay and Lynne Farrow for their contribution to the Elf5 immunohistochemical analysis of patient samples, Dr Simon Junankar for his technical advice for the FACS analysis of immune populations, Mr Henry Hampton for his technical advice with the Ly6G-neutrophil depletion experiments, Dr. Alana L. Welm for the PyMT Q-PCR primer sequences and Ms Gillian Lehrbach, the Australian BioResources (ABR) facility and the Garvan Molecular Genetics staff for their assistance.

Financial Disclosure

This work has been supported by the National Health and Medical Research Council (NHMRC) Australia, Cancer Council New South Wales (NSW), National Breast Cancer Foundation Australia, Cancer Institute NSW, Banque Nationale de Paris Paribas Australia, RT Hall Trust and Breast Cancer Campaign UK. DGO and FVM are Fellows of the National Breast Cancer Foundation and

Cure Cancer Foundation Australia. SRO is a Fellow of the National Breast Cancer Foundation. JMWG is a Breast Cancer Campaign Fellow. The funders had no role in study design, data collection and analysis, decision to publish, or preparation of the manuscript

References

1. Curtis C, Shah SP, Chin SF, Turashvili G, Rueda OM, et al. (2012) The genomic and transcriptomic architecture of 2,000 breast tumours reveals novel subgroups. Nature 486: 346-352.

2. Fisher B, Redmond C, Fisher ER, Caplan R (1988) Relative worth of estrogen or progesterone receptor and pathologic characteristics of differentiation as indicators of prognosis in node negative breast cancer patients: findings from National Surgical Adjuvant Breast and Bowel Project Protocol B-06. J Clin Oncol 6: 1076-1087.

3. Bentzon N, During M, Rasmussen BB, Mouridsen H, Kroman N (2008) Prognostic effect of estrogen receptor status across age in primary breast cancer. Int J Cancer 122: 1089-1094.

4. Maehara Y, Emi Y, Sakaguchi Y, Kusumoto T, Kakeji Y, et al. (1990) Estrogen-receptor-negative breast cancer tissue is chemosensitive in vitro compared with estrogen-receptor-positive tissue. Eur Surg Res 22: 50-55.

5. Rouzier R, Perou CM, Symmans WF, Ibrahim N, Cristofanilli M, et al. (2005) Breast cancer molecular subtypes respond differently to preoperative chemotherapy. Clin Cancer Res 11: 5678-5685.

6. Colleoni M, Viale G, Zahrieh D, Pruneri G, Gentilini O, et al. (2004) Chemotherapy is more effective in patients with breast cancer not expressing steroid hormone receptors: a study of preoperative treatment. Clin Cancer Res 10: 6622-6628.

7. Visvader JE, Stingl J (2014) Mammary stem cells and the differentiation hierarchy: current status and perspectives. Genes Dev 28: 1143-1158.

8. Oakes SR, Naylor MJ, Asselin-Labat ML, Blazek KD, Gardiner-Garden M, et al. (2008) The Ets transcription factor Elf5 specifies mammary alveolar cell fate. Genes Dev 22: 581-586.

9. Gallego-Ortega D, Oakes SR, Lee HJ, Piggin CL, Ormandy CJ (2013) ELF5, normal mammary development and the heterogeneous phenotypes of breast cancer. Breast Cancer Management 2: 489-498.

10. Oakes SR, Gallego-Ortega D, C.J. O (2014) The mammary cellular hierarchy and breast cancer. Cellular and Molecular Life Sciences In press.

11. Chakrabarti R, Hwang J, Andres Blanco M, Wei Y, Lukacisin M, et al. (2012) Elf5 inhibits the epithelial-mesenchymal transition in mammary gland development and breast cancer metastasis by transcriptionally repressing Snail2. Nat Cell Biol 14: 1212-1222.

12. Lee HJ, Hinshelwood RA, Bouras T, Gallego-Ortega D, Valdes-Mora F, et al. (2011) Lineage specific methylation of the Elf5 promoter in mammary epithelial cells. Stem Cells 29: 1611-1619.

13. Lee HJ, Gallego-Ortega D, Ledger A, Schramek D, Joshi P, et al. (2013) Progesterone drives mammary secretory differentiation via RankL-mediated induction of Elf5 in luminal progenitor cells. Development 140: 1397-1401.

14. Harris J, Stanford PM, Sutherland K, Oakes SR, Naylor MJ, et al. (2006) Socs2 and elf5 mediate prolactin-induced mammary gland development. Mol Endocrinol 20: 1177-1187.

15. Brisken C, Heineman A, Chavarria T, Elenbaas B, Tan J, et al. (2000) Essential function of Wnt-4 in mammary gland development downstream of progesterone signaling. Genes Dev 14: 650-654.

16. Rios AC, Fu NY, Lindeman GJ, Visvader JE (2014) In situ identification of bipotent stem cells in the mammary gland. Nature 506: 322-327.

17. Kalyuga M, Gallego-Ortega D, Lee HJ, Roden DL, Cowley MJ, et al. (2012) ELF5 suppresses estrogen sensitivity and underpins the acquisition of antiestrogen resistance in luminal breast cancer. PLoS Biol 10: e1001461.

18. Guy CT, Cardiff RD, Muller WJ (1992) Induction of mammary tumors by expression of polyomavirus middle T oncogene: a transgenic mouse model for metastatic disease. Mol Cell Biol 12: 954-961.

19. Lin EY, Jones JG, Li P, Zhu L, Whitney KD, et al. (2003) Progression to malignancy in the polyoma middle T oncoprotein mouse breast cancer model provides a reliable model for human diseases. Am J Pathol 163: 2113-2126.

20. Maglione JE, Moghanaki D, Young LJ, Manner CK, Ellies LG, et al. (2001) Transgenic Polyoma middle-T mice model premalignant mammary disease. Cancer Res 61: 8298-8305.

21. Trimboli AJ, Fukino K, de Bruin A, Wei G, Shen L, et al. (2008) Direct evidence for epithelial-mesenchymal transitions in breast cancer. Cancer Res 68: 937-945.

22. Lin EY, Nguyen AV, Russell RG, Pollard JW (2001) Colony-stimulating factor 1 promotes progression of mammary tumors to malignancy. J Exp Med 193: 727-740.

23. Ishihara D, Dovas A, Hernandez L, Pozzuto M, Wyckoff J, et al. (2013) Wiskott-Aldrich syndrome protein regulates leukocyte-dependent breast cancer metastasis. Cell Rep 4: 429-436.

24. Gabrilovich DI, Ostrand-Rosenberg S, Bronte V (2012) Coordinated regulation of myeloid cells by tumours. Nat Rev Immunol 12: 253-268.

25. Melani C, Chiodoni C, Forni G, Colombo MP (2003) Myeloid cell expansion elicited by the progression of spontaneous mammary carcinomas in c-erbB-2 transgenic BALB/c mice suppresses immune reactivity. Blood 102: 2138-2145.

26. Young MR, Lathers DM (1999) Myeloid progenitor cells mediate immune suppression in patients with head and neck cancers. Int J Immunopharmacol 21: 241-252.

27. Yang L, DeBusk LM, Fukuda K, Fingleton B, Green-Jarvis B, et al. (2004) Expansion of myeloid immune suppressor Gr+CD11b+ cells in tumor-bearing host directly promotes tumor angiogenesis. Cancer Cell 6: 409-421.

28. Liu C, Yu S, Kappes J, Wang J, Grizzle WE, et al. (2007) Expansion of spleen myeloid suppressor cells represses NK cell cytotoxicity in tumor-bearing host. Blood 109: 4336-4342.

29. Kusmartsev S, Nefedova Y, Yoder D, Gabrilovich DI (2004) Antigen-specific inhibition of CD8+ T cell response by immature myeloid cells in cancer is mediated by reactive oxygen species. J Immunol 172: 989-999.

30. Joyce JA, Pollard JW (2009) Microenvironmental regulation of metastasis. Nat Rev Cancer 9: 239-252.

31. Li Z, Pang Y, Gara SK, Achyut BR, Heger C, et al. (2012) Gr-1+CD11b+ cells are responsible for tumor promoting effect of TGF-beta in breast cancer progression. Int J Cancer 131: 2584-2595.

32. Yang L, Huang J, Ren X, Gorska AE, Chytil A, et al. (2008) Abrogation of TGF beta signaling in mammary carcinomas recruits Gr-1+CD11b+ myeloid cells that promote metastasis. Cancer Cell 13: 23-35.

33. Gunther EJ, Belka GK, Wertheim GB, Wang J, Hartman JL, et al. (2002) A novel doxycycline-inducible system for the transgenic analysis of mammary gland biology. FASEB J 16: 283-292.

34. Lim E, Vaillant F, Wu D, Forrest NC, Pal B, et al. (2009) Aberrant luminal progenitors as the candidate target population for basal tumor development in BRCA1 mutation carriers. Nature medicine 15: 907-913.

35. Habashy HO, Powe DG, Staka CM, Rakha EA, Ball G, et al. (2010) Transferrin receptor (CD71) is a marker of poor prognosis in breast cancer and can predict response to tamoxifen. Breast Cancer Res Treat 119: 283-293.

36. Goldhirsch A, Wood WC, Coates AS, Gelber RD, Thurlimann B, et al. (2011) Strategies for subtypes--dealing with the diversity of breast cancer: highlights of the St. Gallen International Expert Consensus on the Primary Therapy of Early Breast Cancer 2011. Ann Oncol 22: 1736-1747.

37. Galea MH, Blamey RW, Elston CE, Ellis IO (1992) The Nottingham Prognostic Index in primary breast cancer. Breast Cancer Res Treat 22: 207-219.

38. Sheen-Chen SM, Hsu W, Eng HL, Huang CC, Ko SF (2007) Intratumoral hemorrhage of mammary phyllodes tumor after menstrual induction: a puzzling presentation. Tumori 93: 631-633.

39. Irizarry RA, Bolstad BM, Collin F, Cope LM, Hobbs B, et al. (2003) Summaries of Affymetrix GeneChip probe level data. Nucleic Acids Research 31: 15e-15.

40. Gautier L, Cope L, Bolstad BM, Irizarry Ra (2004) affy--analysis of Affymetrix GeneChip data at the probe level. Bioinformatics (Oxford, England) 20: 307-315.

41. Gentleman RC, Carey VJ, Bates DM, Bolstad B, Dettling M, et al. (2004) Bioconductor: open software development for computational biology and bioinformatics. Genome biology 5: R80.

42. Subramanian A, Tamayo P, Mootha VK, Mukherjee S, Ebert BL, et al. (2005) Gene set enrichment analysis: a knowledge-based approach for interpreting genome-wide expression profiles. Proceedings of the National Academy of Sciences of the United States of America 102: 15545-15550.

43. Reich M, Liefeld T, Gould J, Lerner J, Tamayo P, et al. (2006) GenePattern 2.0. Nat Genet 38: 500-501.

44. Koboldt DC, Fulton RS, McLellan MD, Schmidt H, Kalicki-Veizer J, et al. (2012) Comprehensive molecular portraits of human breast tumours. Nature advance on.

45. Smyth GK (2004) Linear models and empirical bayes methods for assessing differential expression in microarray experiments. Statistical applications in genetics and molecular biology 3: Article3.

46. Liberzon A, Subramanian A, Pinchback R, Thorvaldsdóttir H, Tamayo P, et al. (2011) Molecular signatures database (MSigDB) 3.0. Bioinformatics (Oxford, England) 27: 1739-1740.

47. Shannon P, Markiel A, Ozier O, Baliga NS, Wang JT, et al. (2003) Cytoscape: a software environment for integrated models of biomolecular interaction networks. Genome research 13: 2498-2504.

48. Merico D, Isserlin R, Stueker O, Emili A, Bader GD (2010) Enrichment map: a network-based method for gene-set enrichment visualization and interpretation. PloS one 5: e13984.

49. Prat A, Parker JS, Karginova O, Fan C, Livasy C, et al. (2010) Phenotypic and molecular characterization of the claudin-low intrinsic subtype of breast cancer. Breast Cancer Res 12: R68.

50. Livak KJ, Schmittgen TD (2001) Analysis of relative gene expression data using real-time quantitative PCR and the 2(-Delta Delta C(T)) Method. Methods 25: 402-408.

51. Gray DC, Hoeflich KP, Peng L, Gu Z, Gogineni A, et al. (2007) pHUSH: a single vector system for conditional gene expression. BMC Biotechnol 7: 61.

Figure legends

Figure 1. ELF5 produces hemorrhagic mammary tumors.

Panel A, the promoter from the mouse mammary tumor virus (pMMTV) drives expression of the reverse tetracycline transactivator (rtTA), which binds doxycycline to activate the tetracycyline-on promoter (pTetOn), which drives expression of a single mRNA encoding ELF5 and the enhanced Green Fluorescent Protein (EGFP), translated as 2 independent proteins by the presence of an internal ribosome entry site (IRES). The Polyoma Middle T (PyMT) oncogene is constitutively expressed from pMMTV. All alleles are integrated separately in the mouse genome. DOX was administered in either an acute or chronic scenario as indicated. **Panel B**, ELF5 levels in response to DOX administration measured by Western blot. Nsb, non specific band. **Panel C**, appearance of tumors, and the presence of erythrocytes, altered vasculature and hematopoietic cell infiltrate (Arrows) driven by ELF5 (Scale Bars 100μm). **Panel D,** quantification of vessel number and area is shown in the RHS panels, each point is a randomly chosen field. **Panel E,** quantification by flow cytometry of erythrocytes, endothelial cells and hematopoietic cells with the tumors in the acute and chronic scenarios. Each dot is an individual tumor.

Figure 2. Effects of ELF5 on survival.

Panel A, heterogeneous expression of ELF5 within tumours visualized by EGFP expression. **Panel B**, % tumour burden for each experimental group. **Panel C**, Survival analysis of time to ethical endpoint (10% weight gain), time to tumor detection and time from detection to ethical endpoint in animals of the indicated

genotypes carrying tumors that developed *in situ*. **Panel D**, survival analysis in animals of the indicated genotypes carrying tumors that developed from an intraductal transplant of EGFP+ tumor cells following chronic administration of DOX. **Panel E**, survival analysis in animals of the indicated genotypes carrying tumors that developed from intraductal transplantation of EGFP+ tumor cells following 7days administration of DOX, then receiving DOX as indicated. Log-rank p values are shown for +/- DOX comparison. N.S.; not significant.

Figure 3. Effects of ELF5 on cell-autonomous aspects of metastasis.

Panel A and B, BrdU incorporation by cells in S-phase relative to ELF5 levels marked by EGFP expression under acute and chronic conditions of DOX administration respectively. **Panels C and D**, Flow-sorted EGFP+ tumor cells from chronically DOX-treated mice assayed in Boyden chambers for motility through a membrane toward serum containing medium, or for invasion through matrigel first. Panel D right, established ELF5 inducible PyMT cell line. **Panel E**, injection of EGFP+ tumor cells from chronically DOX-treated mice into the tail vein of syngenic WT host animals. Lungs were sectioned, stained with H&E and metastases counted in random fields. **Panels F and G**, SES analysis of shifts in molecular subtype produced by acute or chronic administration of DOX. B; basal, LB; luminal b, H; Her2+, LA; luminal A, N; normal-like, C; claudin-low. **Panel H**, heat map ranked by the t-statistic, showing the change in expression of a set of genes involved in epithelial to mesenchymal transition. **Panel I**, overlap of differentially expressed genes in Panel H.

Figure 4. Effects of ELF5 on metastases to the lungs.

Panel A, appearance of lungs from a control PyMT animal following chronic Dox treatment. **Panel B**, H&E histology of lungs in Panel A. **Panels C and D,** examples of H&E histology of lungs from control PyMT mice receiving acute Dox treatment. **Panel E**, appearance of lungs following chronic ELF5 expression. **Panel F**, H&E histology of the lungs in Panel E. **Panel G and H**, H&E histology of lungs from mice receiving acute induction of ELF5. **Panel I**, visualization of EGFP of the lungs in Panel E. **Panel J**, example of IHC staining for ELF5 in a lung metastasis. **Panel K**, relationship between the size of an individual lung lesion and the IHC score for ELF5 level (combining intensity and %positivity). **Panel L and M**, quantification of the number of metastases in the lungs of the mice with the indicated genotypes in either chronic or acute scenarios. **Panel N**, comparison to the number of metastases driven by pregnancy. **Panel O**, metastatic behavior of the indicated genotypes expressed as an area. **Panel P,** PyMT expression measured by PCR in circulating tumor cells in the blood of mice of the indicated genotypes, isolated by flow cytometry using CD24.

Figure 5. Patterns of gene expression driven by ELF5 in primary tumours, and comparison to subsequent changes in gene expression following metastasis.

Cytoscape visulalization of the changes in gene set enrichment in primary tumors (inner node colour) compared to the changes occurring in lung metastases (outer node color). Labels summarize the functions of gene set clusters indicated by grey shading. Red node color indictaes positive gene set enrichment and augmentation of function. Blue node color indicates negative enrichment and the suppression of function. **Inset, top LHS**, SES analysis of

change in molecular subtype of lung metastases compared to primary mammary tumors. Heat map at the bottom shows the expression of the EMT signature from Figure 3, using the same scale and coloring in primary tumours (Pri.) compared to lung metastases (Met.).

Figure 6. Immune cell subsets within tumours and the effect of depletion of MDSCs on ELF5-driven lung metastases.

Panels A and B, tumor content of myeloid or lymphoid linage immune cell subsets expressed as either a proportion of total tumor cells (after erythrocyte lysis) or as a proportion of CD45+ hematopoietic cells. SFig. 6 shows the gating strategy. Mice of the indicated genotypes with established tumors were treated with DOX from 11-12 weeks of age for 2 weeks with or without Ly6G antibody as indicated. **Panel C**, the presence of MDSC in the circulation and tumor was measured by flow cytometry and; **Panel D**, the number of lung metastases was measured by H&E serial sections. **Panel E** shows tumor erythrocyte content in response to the antibody treatment.

Figure 7. Functions correlated with *ELF5* expression in the TCGA series of luminal breast cancers.

Gene expression was correlated with *ELF5* expression in PAM50 defined Luminal A and B breast cancer, and the ranked list (by correlation coefficient) was used as input for GSEA. **Panel A**, the entire network, which can be viewed as a scalable .pdf in sFig 7. **Panel B**, a subnetwork indicated by yellow nodes in panel A. Key shows colors denoting enrichment of the indicated gene sets. **Panel C**, enrichment of lactation and involution signatures in the PyMT mouse model in

response to induction of ELF5, and in the TCGA series of luminal breast cancer correlated with *ELF5* expression. **Panel C**, gives the t-statistic for the indicated human or mouse samples, red for significantly enriched, blue for significantly suppressed, grey not statistically significant.

Figure 8. Elf5 immunohistochemistry as a predictor of luminal breast cancer survival.

ELF5 was measured by immunohistochemistry in the cytoplasm and nucleus of tumors in a subset of ER+ samples from the Nottingham breast cancer series. **Panel A**, overall survival (OS) and **Panel B** distant metastasis free survival (DMFS). Hazards ratio (HR) and Log Rank p value (LRp) are given. Tumors are split into high ELF5 expression (green) and low Elf5 expression (blue) by XTile.

Supplementary Figure Legends

sFigure 1. Forced ELF5 expression induces a mesenchymal to epithelial transition in the highly mesenchymal and metastatic cell line MDA-MB-231.

Panel A, construction of a DOX-inducible ELF5 expression model in MDA-MB-231 and derivation of clonal lines from pools of stably-transfected cells. **Panel B**, cell growth habits in response to induction of ELF5. **Panel C**, The effect of ELF5 expression on cell accumulation rates during culture. **Panel D,** expression of markers of mesenchymal to epithelial transition in response to induction of ELF5, **Panel E**, Effect of ELF5 on rates of monolayer wound closure in a scratch assay. **Panels F and G**, Effect of ELF5 expression in Boyden chamber assays for motility through a membrane toward serum containing medium, or for invasion through matrigel first. **Panel H**, injection MDA-MB-231 cells into the tail vein of Rag1-/- host animals. Growth of lung metastases were monitored by luciferase.

Supplementary Figure 2. GSEA representation of gene expression changes produced by acute or chronic expression of ELF5.

Figure can be viewed at a range of high magnifications, 1600% or higher, to identify individual gene sets and to see the composition of functional clusters.

Supplementary Figure 3. GSEA representation stem and progenitor gene expression changes produced by acute or chronic expression of ELF5.

Subnetwork from Supplementary Figure 2, indicated by the yellow nodes in the outline network at the top LHS, showing differential enrichment of stem cell sets forming a functional cluster.

Supplementary Figure 4. GSEA representation of differential gene expression produced by chronic induction of ELF5 in primary mammary tumors compared to lung metastases occurring during chronic induction of ELF5.

Figure can be viewed at a range of high magnifications, 1600% or higher, to identify individual gene sets and to see the composition of functional clusters.

Supplementary Figure 5. GSEA subnetwork of differential gene expression produced by chronic induction of ELF5 in primary mammary tumors compared to lung metastases occurring during chronic induction of ELF5.

Subnetwork from Supplementary Figure 4, indicated by the yellow nodes in the outline network at the top LHS, showing functional clusters indicative of breast cancer phenotype.

Supplementary Figure 6. Gating strategy used to isolate MDSCs and other immune cell subsets from PyMT tumors.

Data in Figure 5 was produced by flow cytometry using this series of gated cell populations and the indicated antibodies. Color coding of antibodies shows the gated populations they selected.

Supplementary Figure 7. GSEA representation of patterns of gene expression correlated with ELF5 expression in luminal A and B breast cancers from the TCGA series.

Figure can be viewed at a range of high magnifications, 1600% or higher, to identify individual gene sets and to see the composition of functional clusters.

Supplementary Figure 8. MDSC regulators are changed in PyMT mouse mammry cancer and luminal A breast cancer in response to ELF5 expression.

Panel A, Expression of regulators of MDSC by PyMT tumors in response to acute and chronic induction of ELF5 expression. **Panel B**, PyMT tumors respond to the most differentially regulated MDSC factors in PyMT tumours. **Panel C**, enrichment of gene sets indicating activity of ELF5-regulated MDSCs factors, by correlation to ELF5 expression in luminal breast cancers from the TCGA series.

Supplementary Table 1

Pheotypic characteristic	Cytoplasmic ELF5	Nuclear ELF5	Stat. test
ER+ patients			
higher in local recurrence	NS	p=0.025	Mann Whitney
higher in regional recurrence	NS	p=0.013	Mann Whitney
distant recurrence	NS	NS	Mann Whitney
higher in Poorer outcome NPI	p=0.048	NS	Mann Whitney
higher in Lobular tumours	p=0.031	NS	Mann Whitney
higher in MIB1 low proliferation	NS	p=0.016	Mann Whitney
higher in lower mitosis		p=0.091	Mann Whitney
higher in higher mitosis	p=0.051		Mann Whitney
higher in Increased tubular differentiation	NS	p=0.075	Mann Whitney
higher in low ER staining	p=0.046		Mann Whitney
higher in ER+ patients		p<0.001	Mann Whitney
ER staining	p=0.032 inverse corr.		Spearman
PR staining	NS	0.068 direct	Spearman

		corr.	
E-Cadherin	p=0.046 inverse corr.	p=0.084 inverse corr.	Spearman
Her3	p=0.089 inverse corr.		Spearman
Cytokeratin19	p=0.063 inverse corr.	p=0.015 direct corr.	Spearman
Cytokeratin 7/8	p=0.099 inverse corr.		Spearman
p53%	p=0.057 direct corr.		Spearman
phosph SRC	p=0.051 direct corr.		Spearman
MIB1	NS	p=0.001 inverse corr	Spearman
Elf5 cytoplasmic	-	p=0.044 direct corr.	Spearman

Legend Supplementary Table 1. Correlations between ELF5 and the indicated prognostic variable within ER+ cancers from the Nottingham cohort, with p value and statistical test used.

Figure 1
Click here to download high resolution image

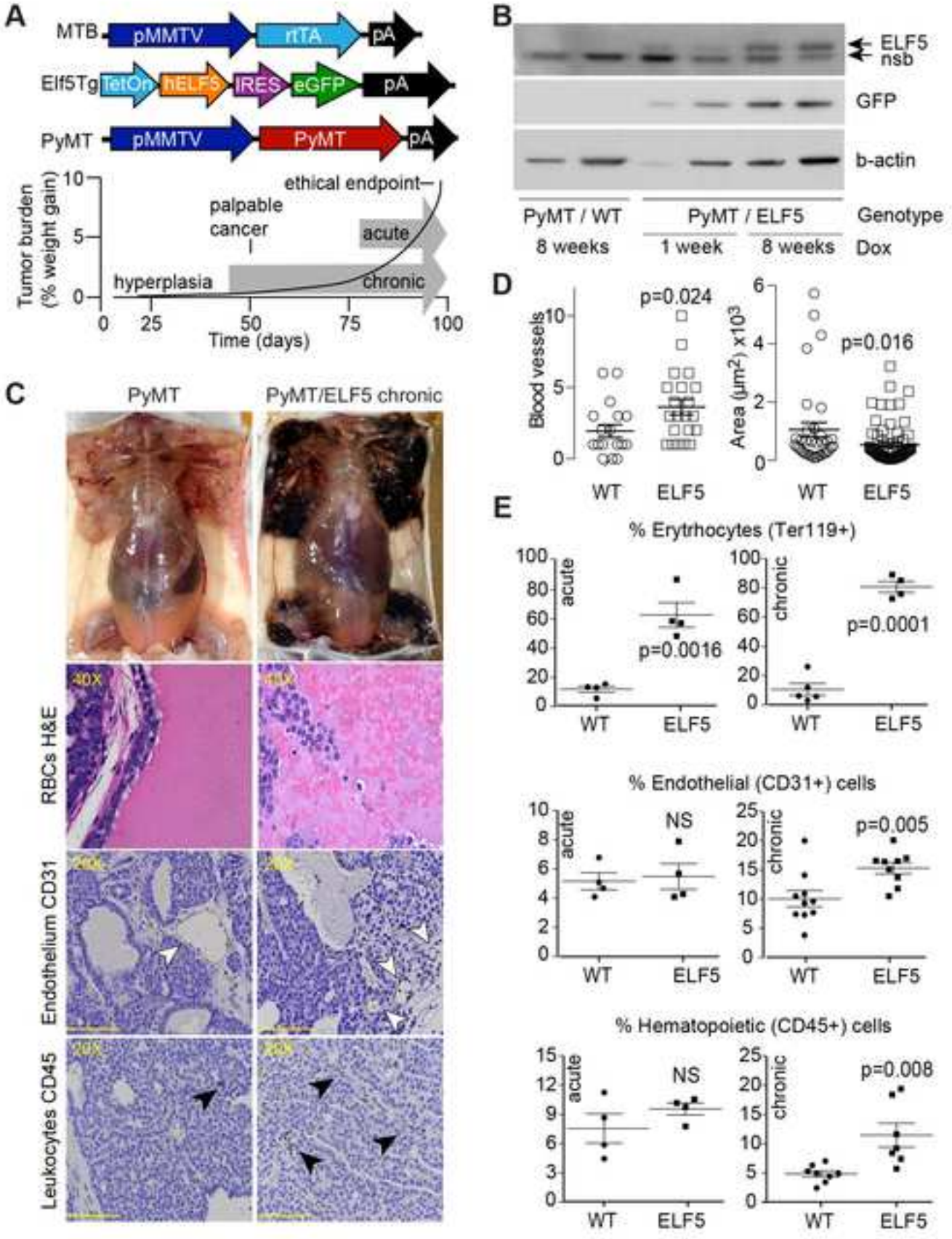

Figure 1. Gallego-Ortega et al.

Figure 2
Click here to download high resolution image

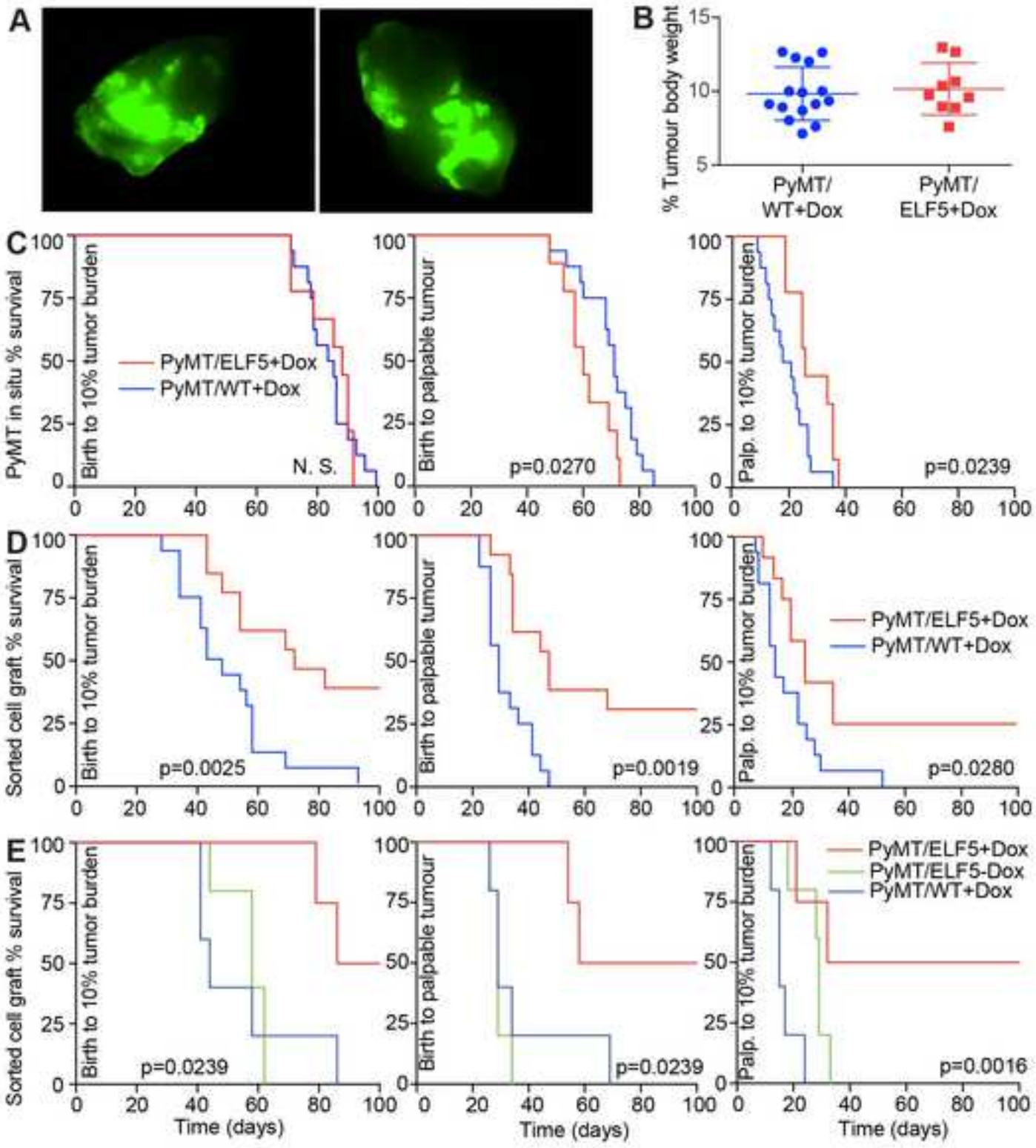

Figure 2. Gallego-Ortega et al.

Figure 3
Click here to download high resolution image

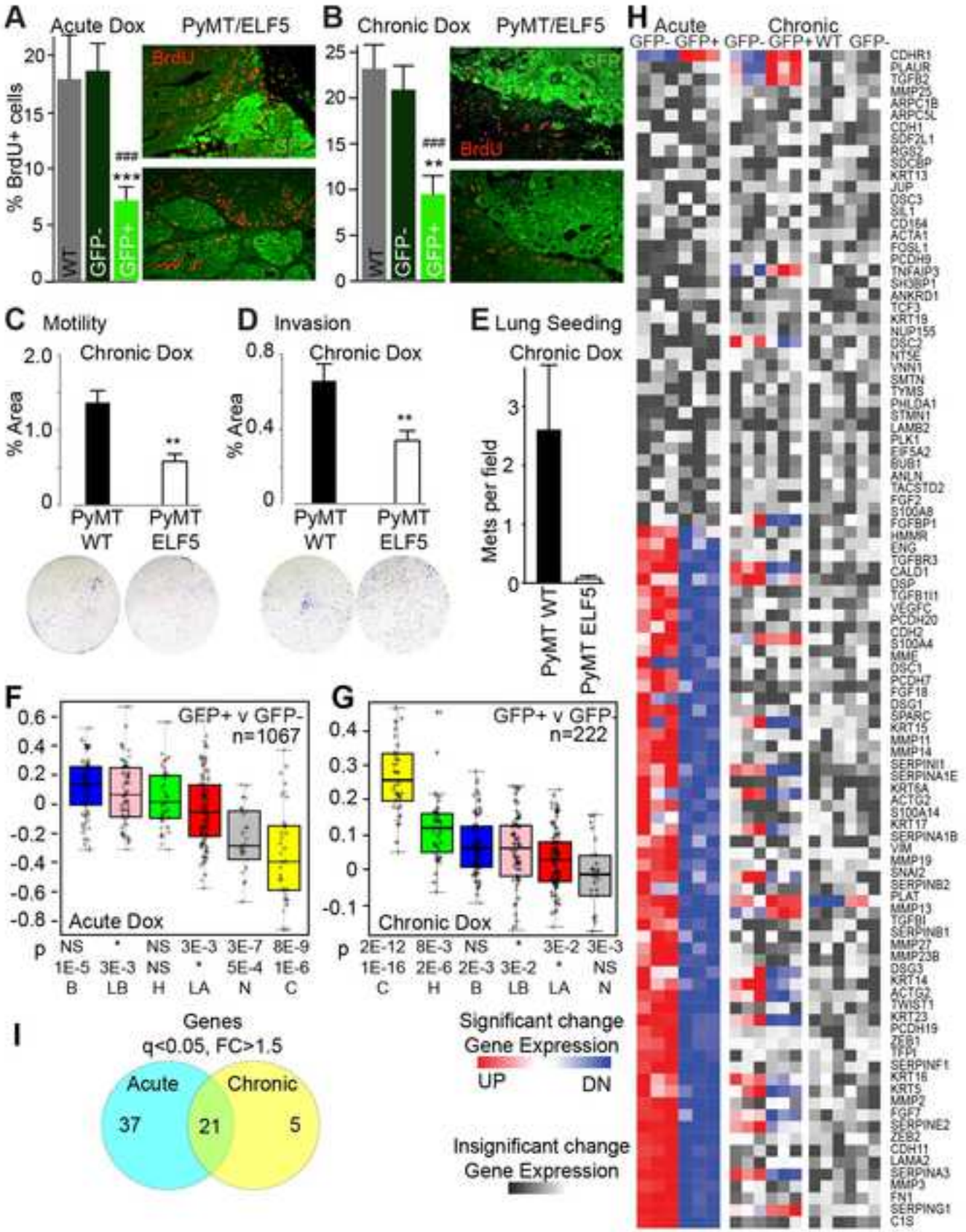

Figure 3 Gallego-Ortega et al.

Figure 4
Click here to download high resolution image

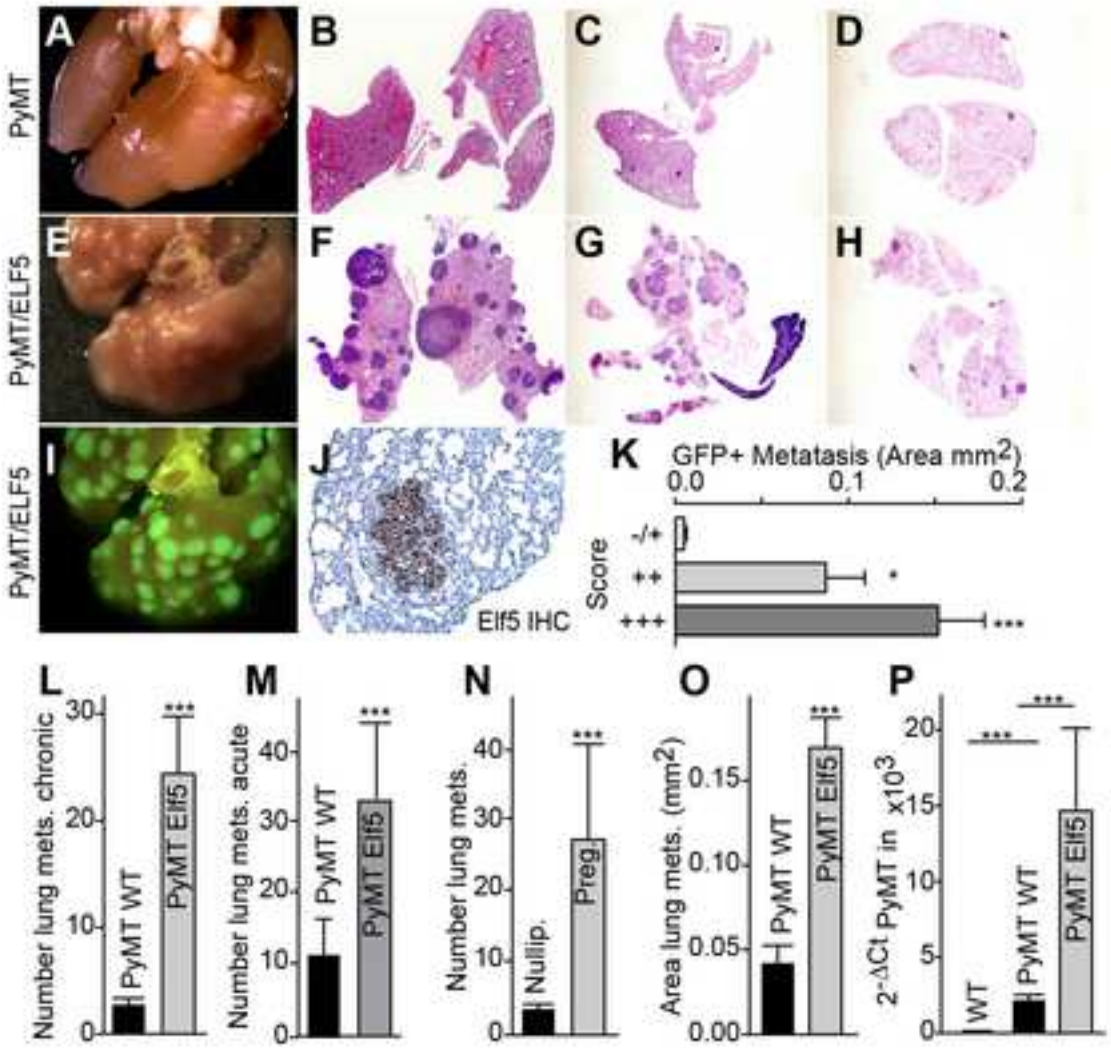

Figure 4 Gallego-Ortega et al.

Figure 5
Click here to download high resolution image

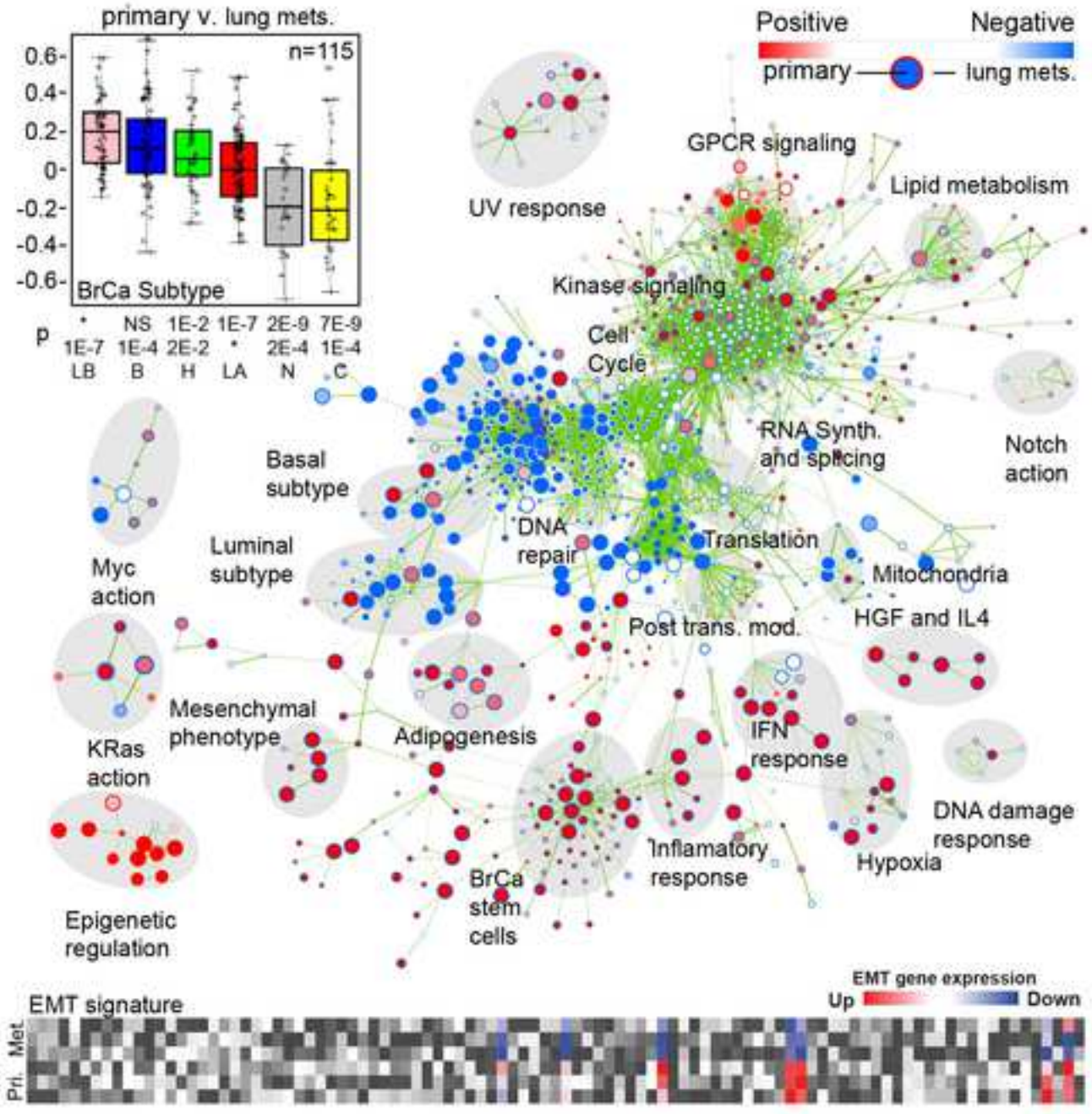

Figure 5 Gallego-Ortega et al.

Figure 6
Click here to download high resolution image

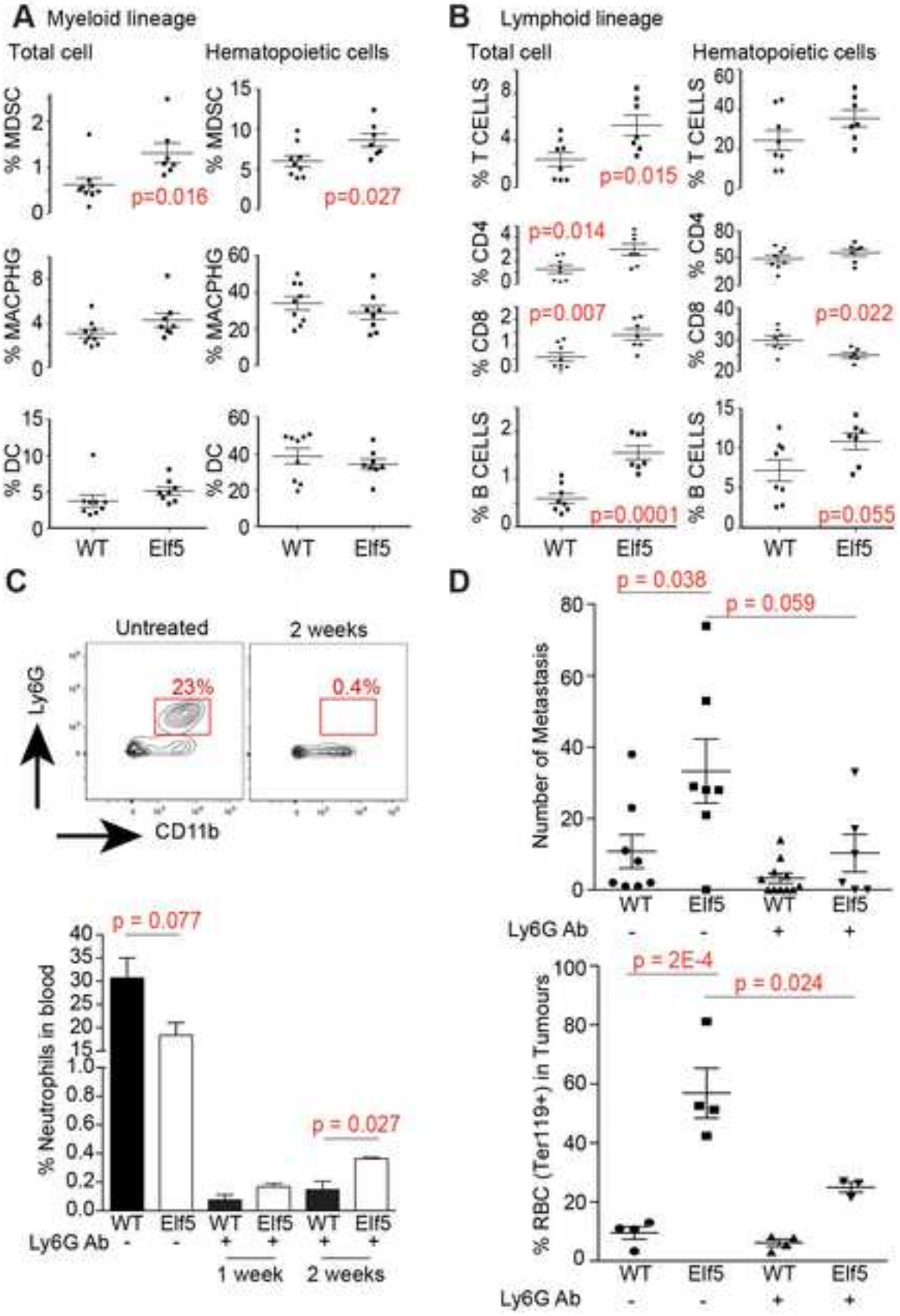

Figure 6 Gallego-Ortega et al.

Figure 7
Click here to download high resolution image

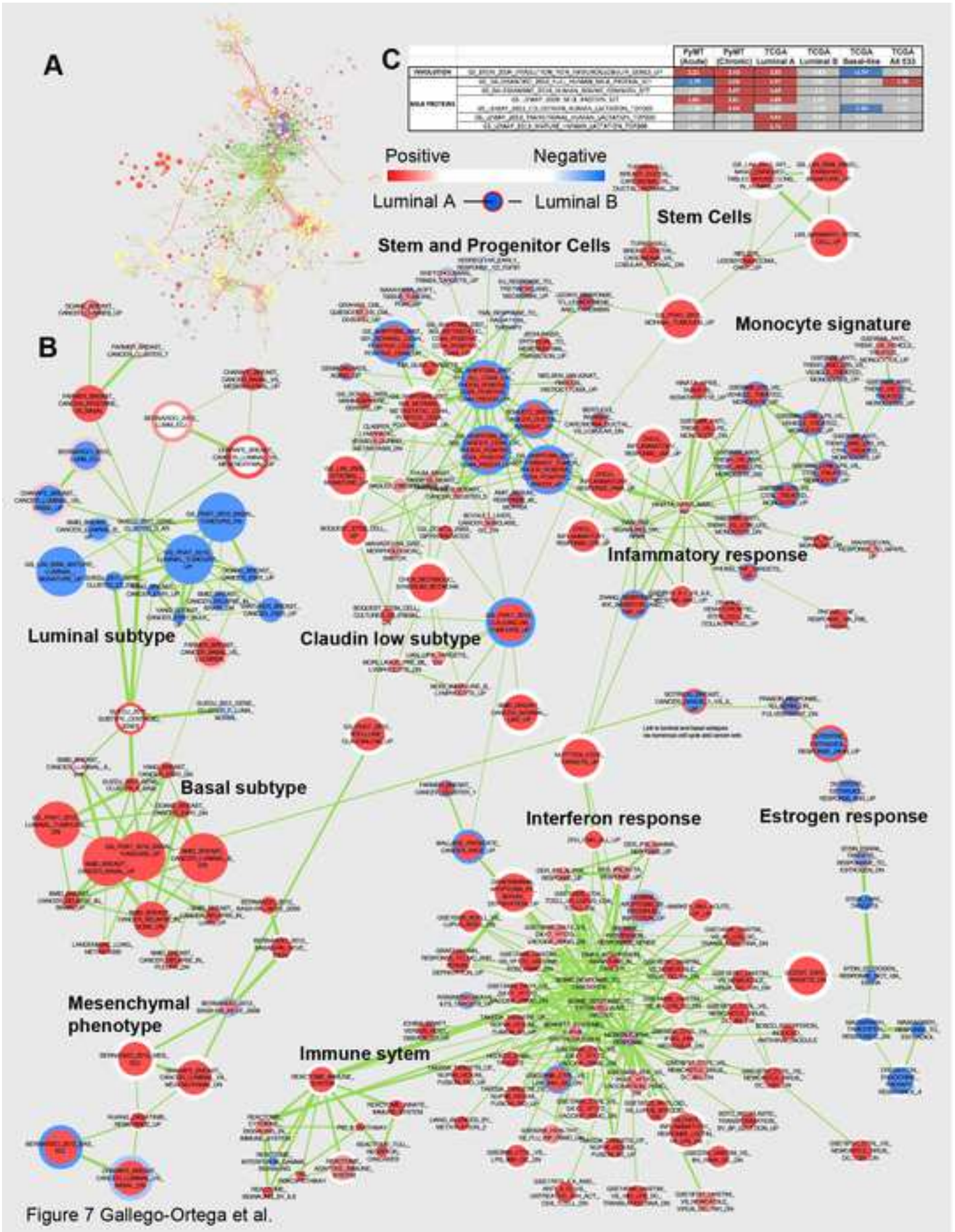

Figure 7 Gallego-Ortega et al.

Figure 8
Click here to download high resolution image

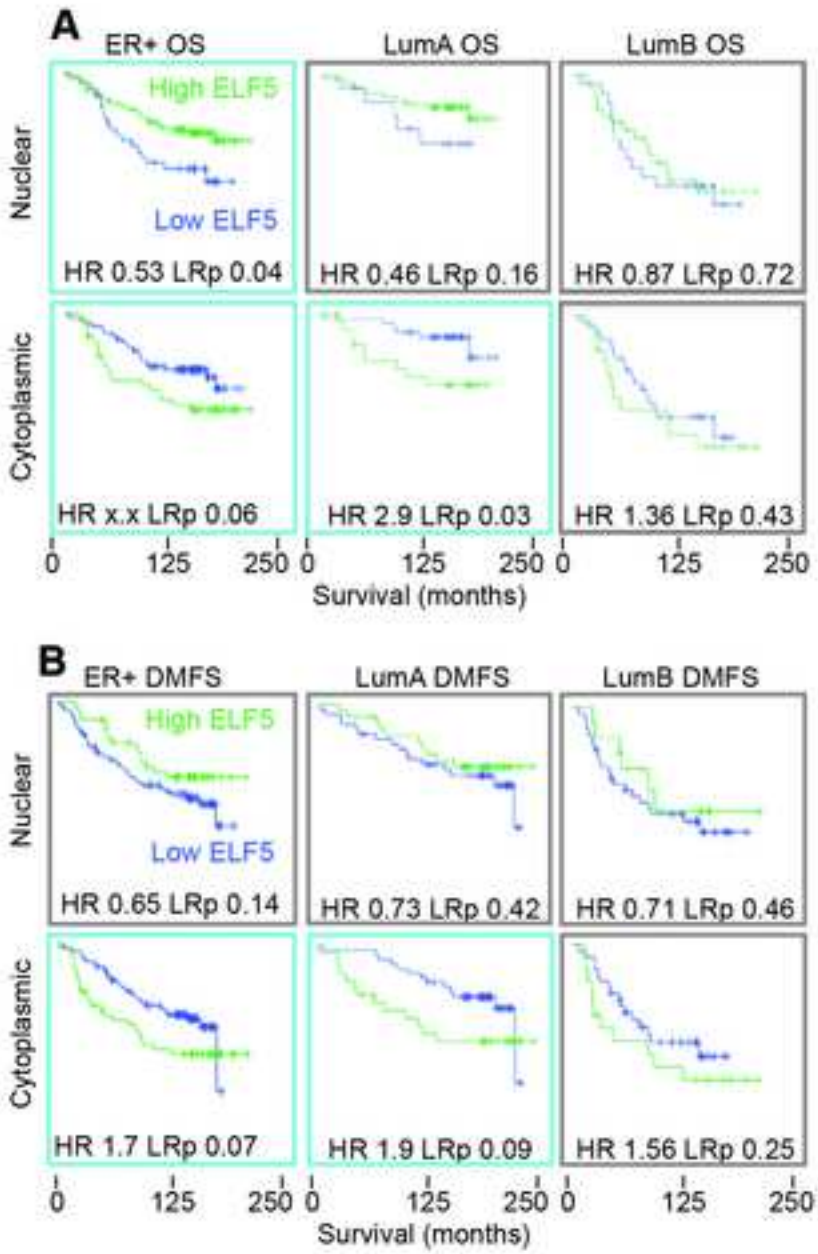

Figure 8 Gallego-Ortega et al.

Supplementary Figure 1
Click here to download Supporting Information: sFig1MDA231.tiff

Supplementary Figure 2 scalable pdf
Click here to download Supporting Information: sFig2acutevchronicCytoscapeFull.pdf

Supplementary Figure 3
Click here to download Supporting Information: sFig3Shipitsin.tiff

Supplementary Figure 4 scalable pdf

Click here to download Supporting Information: sFig4DoxLTvWTvDoxLTMetsCytoFull49222-49237.pdf

Supplementary Figure 5
Click here to download Supporting Information: sFig5PrimaryMetsSubtypeInflam.tiff

Supplementary Figure 6
Click here to download Supporting Information: sFig6GatingStrategy.tiff

Supplementary Figure 7 scalable pdf

Click here to download Supporting Information: sFig7TCGAlumA49593lumB49598.pdf

Supplementary Figure 8
Click here to download Supporting Information: sFig8MDSCpaths.tiff

Elf5 Metastasis

Click here to download high resolution image